

Compressible Magnetohydrodynamic Turbulence: mode coupling, scaling relations, anisotropy, viscosity-damped regime, and astrophysical implications

Jungyeon Cho,^{1*} and A. Lazarian^{2†}

Astronomy Department, University of Wisconsin-Madison, 475 N. Charter St., Madison, WI 53706, USA

MNRAS, accepted

ABSTRACT

We present numerical simulations and explore scalings and anisotropy of compressible magnetohydrodynamic (MHD) turbulence. Our study covers both gas pressure dominated (high β) and magnetic pressure dominated (low β) plasmas at different Mach numbers. In addition, we present results for superAlfvénic turbulence and discuss in what way it is similar to the subAlfvénic turbulence. We describe a technique of separating different magnetohydrodynamic (MHD) modes (slow, fast and Alfvén) and apply it to our simulations. We show that, for both high and low β cases, Alfvén and slow modes reveal the Kolmogorov $k^{-5/3}$ spectrum and scale-dependent Goldreich-Sridhar anisotropy, while fast modes exhibit $k^{-3/2}$ spectrum and isotropy. We discuss the statistics of density fluctuations arising from MHD turbulence at different regimes. Our findings entail numerous astrophysical implications ranging from cosmic ray propagation to gamma ray bursts and star formation. In particular, we show that the rapid decay of turbulence reported by earlier researchers is not related to compressibility and mode coupling in MHD turbulence. In addition, we show that magnetic field enhancements and density enhancements are marginally correlated. Addressing the density structure of partially ionized interstellar gas on AU scales, we show that the viscosity-damped regime of MHD turbulence that we earlier reported for incompressible flows persists for compressible turbulence and therefore may provide an explanation for those mysterious structures.

Key words: turbulence – ISM: general – MHD

1 INTRODUCTION

Astrophysical turbulence is ubiquitous and it holds the key to many astrophysical processes (star formation, heating of the interstellar medium, properties of accretion disks, cosmic ray transport etc). Therefore understanding of turbulence is a necessary requirement for making further progress along any of those directions. Unlike laboratory turbulence astrophysical turbulence is magnetized and highly compressible.

Turbulence has been studied in the context of the interstellar medium (ISM) and the solar wind. The ISM in the Milky Way and neighboring galaxies is known to be turbulent on scales ranging from AUs to kpc (Armstrong, Rickett & Spangler 1995; Stanimirovic & Lazarian 2001; Deshpande et al. 2000). The solar wind also exhibits small-scale turbulence (Leamon et al. 1998). The measured statistics of fluctuations in the ISM and the solar wind is consistent

with the Kolmogorov turbulence obtained for incompressible unmagnetized fluid. This surprising observational evidence¹ resulted in numerous attempts to use Kolmogorov statistics for practical computations of astrophysical quantities, e.g. cosmic ray scattering. We shall show below that in most cases such sort of calculations brings *erroneous* results.

Why would we expect astrophysical fluids to be turbulent and how can we study astrophysical turbulence? A fluid of viscosity ν gets turbulent when the rate of viscous dissipation, which is $\sim \nu/L^2$ at the energy injection scale L , is

¹ The ambiguities of the data interpretation were frequently quoted to justify ignoring this fact. For instance, electron density fluctuations discussed in Armstrong et al. (1995) provide only indirect evidence for Kolmogorov-type spectrum. However, the solar wind observations are made *in situ* and more difficult to disregard. Moreover, a newly developed statistical technique (Lazarian & Pogosyan 2000) allowed us to measure Kolmogorov type spectrum of velocity fluctuations (see also Lazarian & Esquivel 2003).

* E-mail: cho@astro.wisc.edu
 † E-mail: lazarian@astro.wisc.edu

much smaller than the energy transfer rate $\sim V_L/L$, where V_L is the velocity dispersion at the scale L . The ratio of the two rates is the Reynolds number $Re = V_L L/\nu$. In general, when Re is larger than 10 – 100 the system becomes turbulent. Chaotic structures develop gradually as Re increases, and those with $Re \sim 10^3$ are appreciably less chaotic than those with $Re \sim 10^8$. Observed features such as star forming clouds are very chaotic for $Re > 10^8$. This not only ensures that the fluids are turbulent but also makes it difficult to simulate the turbulence. The currently available 3D simulations for 512 cubes can have Re up to $\sim O(10^3)$ and are limited by their grid sizes. Therefore, it is essential to find “scaling laws” in order to extrapolate numerical calculations ($Re \sim O(10^3)$) to real astrophysical fluids ($Re > 10^8$). We show below that even with its limited resolution, numerics is a great tool for *testing* scaling laws.

Kolmogorov theory provides a scaling law for incompressible *non-magnetized* hydrodynamic turbulence (Kolmogorov 1941). This law is true in the statistical sense and it provides a relation between the relative velocity v_l of fluid elements and their separation l , namely, $v_l \sim l^{1/3}$. An equivalent description is to express spectrum $E(k)$ as a function of wave number k ($\sim 1/l$). The two descriptions are related by $kE(k) \sim v_l^2$. The famous Kolmogorov spectrum is $E(k) \sim k^{-5/3}$. The applications of Kolmogorov theory range from engineering research to meteorology (see Monin & Yaglom 1975) but its astrophysical applications are poorly justified.

Let us consider *incompressible* MHD turbulence first. There have long been understanding that the MHD turbulence is anisotropic² (e.g. Shebalin et al. 1983). A substantial progress has been achieved recently by Goldreich & Sridhar (1995; hereafter GS95) who made an ingenious prediction regarding relative motions parallel and perpendicular to magnetic field \mathbf{B} for incompressible MHD turbulence. The GS95 model envisages a Kolmogorov spectrum of velocity and a scale-dependent anisotropy (see below). These relations have been confirmed numerically (Cho & Vishniac 2000b; Maron & Goldreich 2001; Cho, Lazarian & Vishniac 2002a, hereafter CLV02a; see also CLV03a); they are in good agreement with observed and inferred astrophysical spectra (see CLV03a). A remarkable fact revealed in CLV02a is that fluid motions perpendicular to \mathbf{B} are *identical* to hydrodynamic motions. This provides an essential physical insight into why in some respects MHD turbulence and hydrodynamic turbulence are similar, while in other respects they are different.

The GS95 model considered incompressible MHD, but the real ISM is *highly compressible*. Literature on the properties of compressible MHD is very rich (see CLV03a). Back in 80’s Higdon (1984) theoretically studied density fluctuations in the interstellar MHD turbulence. Matthaeus & Brown (1988) studied nearly incompressible MHD at low Mach number and Zank & Matthaeus (1993) extended it. In an important paper Matthaeus et al. (1996) numerically

explored anisotropy of compressible MHD turbulence. However, those papers do not provide universal scalings of the GS95 type.

Is it feasible to obtain scaling relations for the compressible MHD turbulence? Some hints about effects of compressibility can be inferred from the Goldreich & Sridhar (GS95) seminal paper. A more focused discussion was presented in the Lithwick & Goldreich (2001) paper which deals with electron density fluctuations in the gas pressure dominated plasma, i.e. in high β regime ($\beta \equiv P_{gas}/P_{mag} \gg 1$). Incompressible regime formally corresponds to $\beta \rightarrow \infty$ and therefore it is natural to expect that for $\beta \gg 1$ the GS95 picture would persist. Lithwick & Goldreich (2001) also speculated that for low β plasmas the GS95 scaling of slow modes may be applicable. An important study of MHD modes in compressible low β plasmas is given in Cho & Lazarian (2002; hereafter CL02) where we developed and tested our technique of separating different MHD modes.

In this work, we provide a detailed study of mode coupling and scalings of compressible (fast and slow) and Alfvénic modes in high β , intermediate, and low β plasmas. Our approach is complementary to that employed in direct numerical simulations of astrophysical turbulence. In such simulations, e.g. in those dealing with the interstellar medium (see Vazquez-Semadeni et al. 2000), simulations of particular astrophysical objects, e.g. molecular clouds, are attempted. These simulations provide synthetic maps that can be compared with observations. Our goal is to obtain scaling laws that can also be compared with observations. In §2, we describe our approach to the problem including both simple theoretical considerations/expectations that motivate our study and the numerical technique that we employ. In §3, we present velocity spectra and anisotropies for high and low β plasmas. In §4, we discuss scalings of density and magnetic field. In §5, we present the study of viscosity-damped regime of MHD turbulence in compressible fluid. This study extends our earlier work (Cho, Lazarian, & Vishniac 2002b, henceforth CLV02b) where this regime was reported for incompressible flows. In §6, we discuss astrophysical implications of our results, including the rate of MHD turbulence decay, relation between the decay rate and compressibility, correlation of density and magnetic field, and formation of density structures at AU scale. The summary is given in §7.

2 OUR APPROACH

2.1 Theoretical Considerations

Let us start with a discussion why isotropic Kolmogorov turbulence *cannot* be applicable for describing strongly magnetized gas. Assume that, at some large scale L , the magnetic energy and kinetic energy are equal: $\rho V_L^2/2 \sim B^2/(4\pi)$. According to the Kolmogorov theory, the kinetic energy at scale $l < L$ is $\rho V_l^2/2 \sim (l/L)^{2/3}(\rho V_L^2/2)$, which is smaller than the large scale kinetic energy by a factor of $(l/L)^{2/3}$. But, magnetic energy density does not diminish as the scale reduces. Therefore, at scales smaller than L , hydrodynamic motions will not be able to bend magnetic field lines substantially.

An important observation that leads to understanding of the GS95 scaling is that magnetic field cannot pre-

² It is not possible to cite all the important papers in the area of MHD turbulence. An incomplete list of the references in a recent review on the statistics of MHD turbulence by Cho, Lazarian & Vishniac (2003a; henceforth CLV03a) includes about two hundred entries.

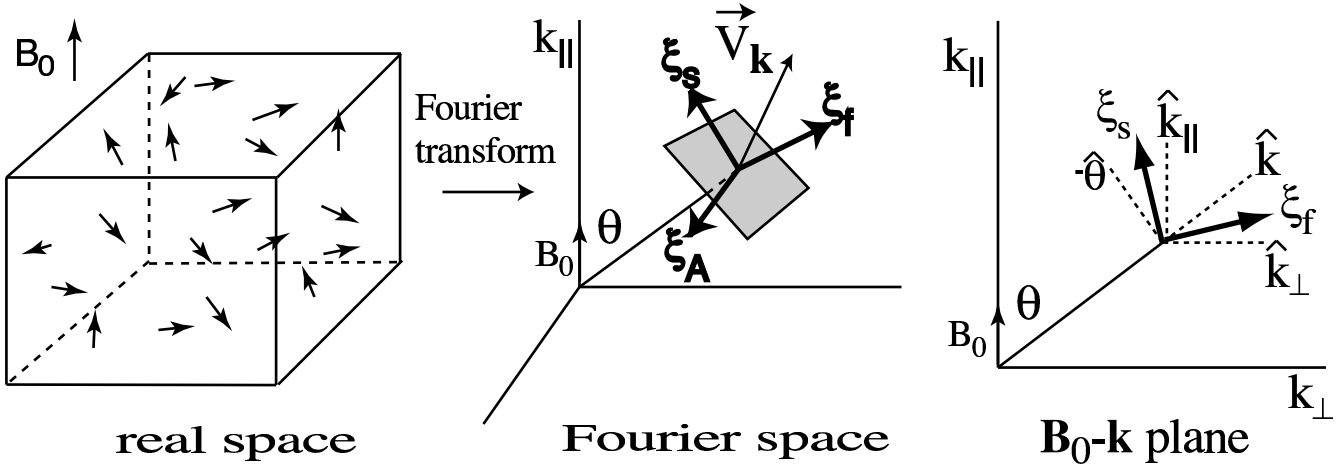


Figure 1. Separation method. We separate Alfvén, slow, and fast modes in Fourier space by projecting the velocity Fourier component $\mathbf{v}_{\mathbf{k}}$ onto bases ξ_A , ξ_s , and ξ_f , respectively. Note that $\xi_A = -\hat{\varphi}$. Slow basis ξ_s and fast basis ξ_f lie in the plane defined by \mathbf{B}_0 and \mathbf{k} . Slow basis ξ_s lies between $-\hat{\theta}$ and $\hat{\mathbf{k}}_{\parallel}$. Fast basis ξ_f lies between $\hat{\mathbf{k}}$ and $\hat{\mathbf{k}}_{\perp}$.

vent mixing motions of magnetic field lines if the motions are perpendicular to the magnetic field. Those motions will cause, however, waves that will propagate along magnetic field lines. If that is the case, the time scale of the wave-like motions, i.e. $\sim l_{\parallel}/V_A$, where l_{\parallel} is the characteristic size of the perturbation along the magnetic field and $V_A = B/\sqrt{4\pi\rho}$ is the local Alfvén speed, will be equal to the hydrodynamic time-scale, l_{\perp}/v_l , where l_{\perp} is the characteristic size of the perturbation perpendicular to the magnetic field. The mixing motions are hydrodynamic-like³ and therefore obey Kolmogorov scaling $v_l \propto l_{\perp}^{1/3}$. Combining the two relations above we can get the GS95 anisotropy, $l_{\parallel} \propto l_{\perp}^{2/3}$ (or $k_{\parallel} \propto k_{\perp}^{2/3}$ in terms of wave-numbers). If we interpret l_{\parallel} as the eddy size in the direction of the local⁴ magnetic field and l_{\perp} as that in the perpendicular directions, the relation implies that smaller eddies are more elongated (see Appendix B for illustration of scale-dependent anisotropy).

How is this idealized incompressible model related to the actual, e.g. interstellar, turbulence? Compressible MHD turbulence is a highly non-linear phenomenon and it has been thought that different types of perturbations or modes (Alfvén, slow and fast) in compressible media are strongly coupled. Nevertheless, one may question whether this is true. A remarkable feature of the GS95 model is that Alfvén perturbations cascade to small scales over just one wave period, while the other non-linear interactions require more time. Therefore one might expect that the non-linear interactions with other types of waves should affect Alfvénic cascade only marginally. Moreover, as the Alfvén waves are incompressible,

the properties of the corresponding cascade may not depend on the sonic Mach number.

The generation of compressible motions (i.e. *radial* components in Fourier space) from Alfvénic turbulence is a measure of mode coupling. How much energy in compressible motions is drained from Alfvénic cascade? According to the closure calculations (Bertoglio, Bataille, & Marion 2001; see also Zank & Matthaeus 1993), the energy in compressible modes in *hydrodynamic* turbulence scales as $\sim M_s^2$ if $M_s < 1$. We may conjecture that this relation can be extended to MHD turbulence if, instead of M_s^2 , we use $\sim (\delta V)_A^2/(a^2 + V_A^2)$. (Hereinafter, we define $V_A \equiv B_0/\sqrt{4\pi\rho}$, where B_0 is the mean magnetic field strength.) However, as the Alfvén modes are anisotropic, this formula may require an additional factor. The compressible modes are generated inside the so-called Goldreich-Sridhar cone, which takes up $\sim (\delta V)_A/V_A$ of the wave vector space. The ratio of compressible to Alfvénic energy inside this cone is the ratio given above. If the generated fast modes become isotropic (see below), the diffusion or, “isotropization” of the fast wave energy in the wave vector space increase their energy by a factor of $\sim V_A/(\delta V)_A$. This results in

$$\frac{(\delta V)_{rad}^2}{(\delta V)_A^2} \lesssim \left[\frac{V_A^2 + a^2}{(\delta V)_A^2} \frac{(\delta V)_A}{V_A} \right]^{-1}, \quad (1)$$

where $(\delta V)_{rad}^2$ and $(\delta V)_A^2$ are energy of compressible⁵ and Alfvén modes, respectively. Eq. (1) suggests that the drain of energy from Alfvénic cascade is marginal when the amplitudes of perturbations are weak, i.e. $(\delta V)_A \ll V_A$.

If Alfvén cascade evolves on its own, it is natural to assume that slow modes exhibit the GS95 scaling. Indeed, slow modes in gas pressure dominated environment (high β plasmas) are similar to the pseudo-Alfvén modes in incompressible regime (see GS95; Lithwick & Goldreich 2001). The latter modes do follow the GS95 scaling. In magnetic pressure dominated environments (low β plasmas), slow modes

³ Recent simulations (Cho et al. 2003) suggest that perpendicular mixing is indeed efficient for mean magnetic fields of up to the equipartition value. This corresponds to our earlier result that high order velocity statistics of MHD turbulence in the perpendicular directions is very similar to that of hydrodynamic one (CLV02a).

⁴ The concept of *local* is crucial. The GS95 scalings are obtained only in the local frame of magnetic field, as this is the frame where magnetic field are allowed to be mixed without being opposed by magnetic tension.

⁵ It is possible to show that the compressible modes inside the Goldreich-Sridhar cone are basically fast modes.

are density perturbations propagating with the sound speed a parallel to the mean magnetic field (see equation (A31)). Those perturbations are essentially static for $a \ll V_A$. Therefore Alfvénic turbulence is expected to mix density perturbations as if they were passive scalar. This also induces GS95 spectrum.

The fast waves in low β regime propagate at V_A irrespectively of the magnetic field direction. In high β regime, the properties of fast modes are similar, but the propagation speed is the sound speed a . Thus the mixing motions induced by Alfvén waves should marginally affect the fast wave cascade. It is expected to be analogous to the acoustic wave cascade and hence be isotropic.

For most part of this paper, we shall assume that $\delta V \sim \delta B/\sqrt{4\pi\rho} \sim B_0/\sqrt{4\pi\rho}$, where δB is the r.m.s. strength of the random magnetic field. This is less restrictive than it might appear, since as long as there is some scale l' in the turbulent cascade where $v_{l'} \sim B/\sqrt{4\pi\rho}$ we can take $L = l'$, $V_L = v_{l'}$ and use this model of turbulence for all smaller scales. Suppose that we have a turbulent system initially threaded by a mean magnetic field only. If initially the turbulent energy is larger than the magnetic energy of the mean field, we are in the regime of so-called superAlfvénic turbulence. In this regime the growth of the magnetic field is expected through so called “turbulent dynamo” (see Batchelor 1950; Brandenburg et al. 1996; Cho & Vishniac 2000a). Initially, the growth of magnetic energy is most active at the scale roughly an order of magnitude larger than the dissipation scale and the magnetic spectrum peaks at the scale. As the magnetic energy grows, the magnetic back reaction becomes important at the scale and the peak of the magnetic power spectrum moves to larger scales. Finally, when equipartition between the kinetic and magnetic energy densities occurs at a scale somewhat (factor of 2 or 3) smaller than the kinetic energy peak, turbulence reaches a statistically stationary state. This agrees well with the results of incompressible simulations in Cho & Vishniac (2000a). However, this is not universally accepted idea. For example, Padoan & Nordlund (1999) reported that, in their compressible simulations, the power spectrum of $\rho^{1/2}v$ has a shallower slope than those of velocity and magnetic field, which implies that equipartition between kinetic magnetic energy cannot be reached at small scales. At scales smaller than the equipartition scale, the turbulence becomes subAlfvénic and our earlier considerations should be applicable.

The arguments above suggest that compressible MHD turbulence should demonstrate well defined scaling relations. Below we test those arguments and reveal scaling relations for different β s and Mach numbers.

2.2 Numerical scheme

We use a third-order accurate hybrid essentially non-oscillatory (ENO) scheme (see CL02) to solve the ideal isothermal MHD equations in a periodic box:

$$\partial\rho/\partial t + \nabla \cdot (\rho\mathbf{v}) = 0, \quad (2)$$

$$\partial\mathbf{v}/\partial t + \mathbf{v} \cdot \nabla\mathbf{v} + \rho^{-1}\nabla(a^2\rho) - (\nabla \times \mathbf{B}) \times \mathbf{B}/4\pi\rho = \mathbf{f}, \quad (3)$$

$$\partial\mathbf{B}/\partial t - \nabla \times (\mathbf{v} \times \mathbf{B}) = 0, \quad (4)$$

with $\nabla \cdot \mathbf{B} = 0$ and an isothermal equation of state. Here \mathbf{f} is a random large-scale driving force, ρ is density, \mathbf{v} is the

velocity, and \mathbf{B} is magnetic field. The rms velocity δV is maintained to be approximately unity (in fact $\delta V \sim 0.7$), so that \mathbf{v} can be viewed as the velocity measured in units of the r.m.s. velocity of the system and $\mathbf{B}/\sqrt{4\pi\rho}$ as the Alfvén velocity in the same units. The time t is in units of the large eddy turnover time ($\sim L/\delta V$) and the length in units of L , the scale of the energy injection. The magnetic field consists of the uniform background field and a fluctuating field: $\mathbf{B} = \mathbf{B}_0 + \mathbf{b}$.

For mode coupling studies (Fig. 2), we do *not* drive turbulence. For scaling studies, we drive turbulence solenoidally in Fourier space and use 216^3 points, $V_A = B_0/\sqrt{4\pi\rho} = 1$, and $\rho_0 = 1$. The average rms velocity in statistically stationary state is $\delta V \sim 0.7$.

For our calculations we assume that $B_0/\sqrt{4\pi\rho} \sim \delta B/\sqrt{4\pi\rho} \sim \delta V$. In this case, the sound speed is the controlling parameter and basically two regimes can exist: supersonic and subsonic. Note that supersonic means low-beta and subsonic means high-beta. When supersonic, we consider mildly supersonic (or, mildly low- β) and highly supersonic (or, very low- β)⁶.

2.3 Separation of MHD modes

Three types of waves exist (Alfvén, slow and fast) in compressible magnetized plasma. The slow, fast, and Alfvén bases that denote the direction of displacement vectors for each mode are given by

$$\hat{\xi}_s \propto (-1 + \alpha - \sqrt{D})k_{\parallel}\hat{\mathbf{k}}_{\parallel} + (1 + \alpha - \sqrt{D})k_{\perp}\hat{\mathbf{k}}_{\perp}, \quad (5)$$

$$\hat{\xi}_f \propto (-1 + \alpha + \sqrt{D})k_{\parallel}\hat{\mathbf{k}}_{\parallel} + (1 + \alpha + \sqrt{D})k_{\perp}\hat{\mathbf{k}}_{\perp}, \quad (6)$$

$$\hat{\xi}_A = -\hat{\varphi} = \hat{\mathbf{k}}_{\perp} \times \hat{\mathbf{k}}_{\parallel}, \quad (7)$$

where $D = (1 + \alpha)^2 - 4\alpha \cos\theta$, $\alpha = a^2/V_A^2 = \beta(\gamma/2)$, θ is the angle between \mathbf{k} and \mathbf{B}_0 , and $\hat{\varphi}$ is the azimuthal basis in the spherical polar coordinate system. These are equivalent to the expression in CL02:

$$\hat{\xi}_s \propto k_{\parallel}\hat{\mathbf{k}}_{\parallel} + \frac{1 - \sqrt{D} - \beta/2}{1 + \sqrt{D} + \beta/2} \left[\frac{k_{\perp}}{k_{\perp}} \right]^2 k_{\perp}\hat{\mathbf{k}}_{\perp}, \quad (8)$$

$$\hat{\xi}_f \propto \frac{1 - \sqrt{D} + \beta/2}{1 + \sqrt{D} - \beta/2} \left[\frac{k_{\perp}}{k_{\parallel}} \right]^2 k_{\parallel}\hat{\mathbf{k}}_{\parallel} + k_{\perp}\hat{\mathbf{k}}_{\perp}. \quad (9)$$

(Note that $\gamma = 1$ for isothermal case.)

Slow and fast velocity components can be obtained by projecting velocity Fourier component $\mathbf{v}_{\mathbf{k}}$ onto $\hat{\xi}_s$ and $\hat{\xi}_f$, respectively. In Appendix A, we discuss how to separate slow and fast magnetic modes. We obtain energy spectra using this projection method. When we calculate the structure functions (e.g. for Alfvén velocity) in real space, we first obtain the Fourier components using the projection and, then, we obtain the real space values by performing Fourier transform.

⁶ The terms “mildly” and “highly” are somewhat arbitrary terms. We consider these two supersonic cases to cover a broad range of parameter space. Note that Boldyrev, Nordlund, & Padoan (2002b) recently provided a Mach number dependence study of the compressible MHD turbulence statistics where only two regimes are manifest: essentially incompressible and essentially compressible shock-dominated (with smooth transition at some M_s of order unity).

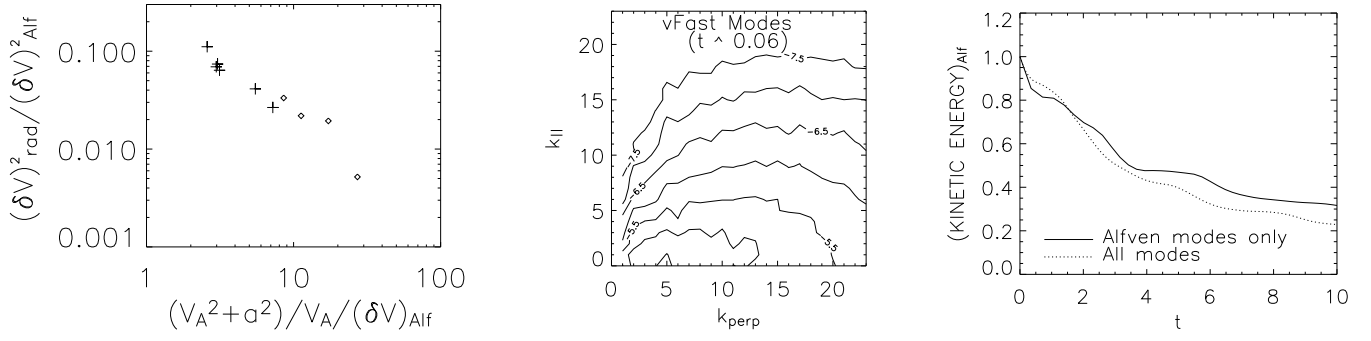


Figure 2. Mode coupling studies. (a) *left*: Square of the r.m.s. velocity of the compressible modes. We use 144^3 grid points. Only Alfvén modes are allowed as the initial condition. “Pluses” are for low β cases ($0.02 \leq \beta \leq 0.4$). “Diamonds” are for high β cases ($1 \leq \beta \leq 20$). (b) *middle*: Generation of fast modes. Snapshot is taken at $t=0.06$ from a simulation (with 144^3 grid points) that started off with Alfvén modes only. Initially, β (ratio of gas to magnetic pressure, P_g/P_{mag}) = 0.2 and M_s (sonic Mach number) ~ 1.6 . (c) *right*: Comparison of decay rates. Decay of Alfvén modes is not much affected by other (slow and fast) modes. We use 216^3 grid points. Initially, $\beta = 0.02$ and $M_s \sim 4.5$ for the solid line and $M_s \sim 7$ for the dotted line. Note that initial data are, in some sense, identical for the solid and the dotted lines. The sonic Mach number for the solid line is smaller because we removed fast and slow modes from the initial data before the decay simulation. For the dotted line, we did *not* remove any modes from the initial data.

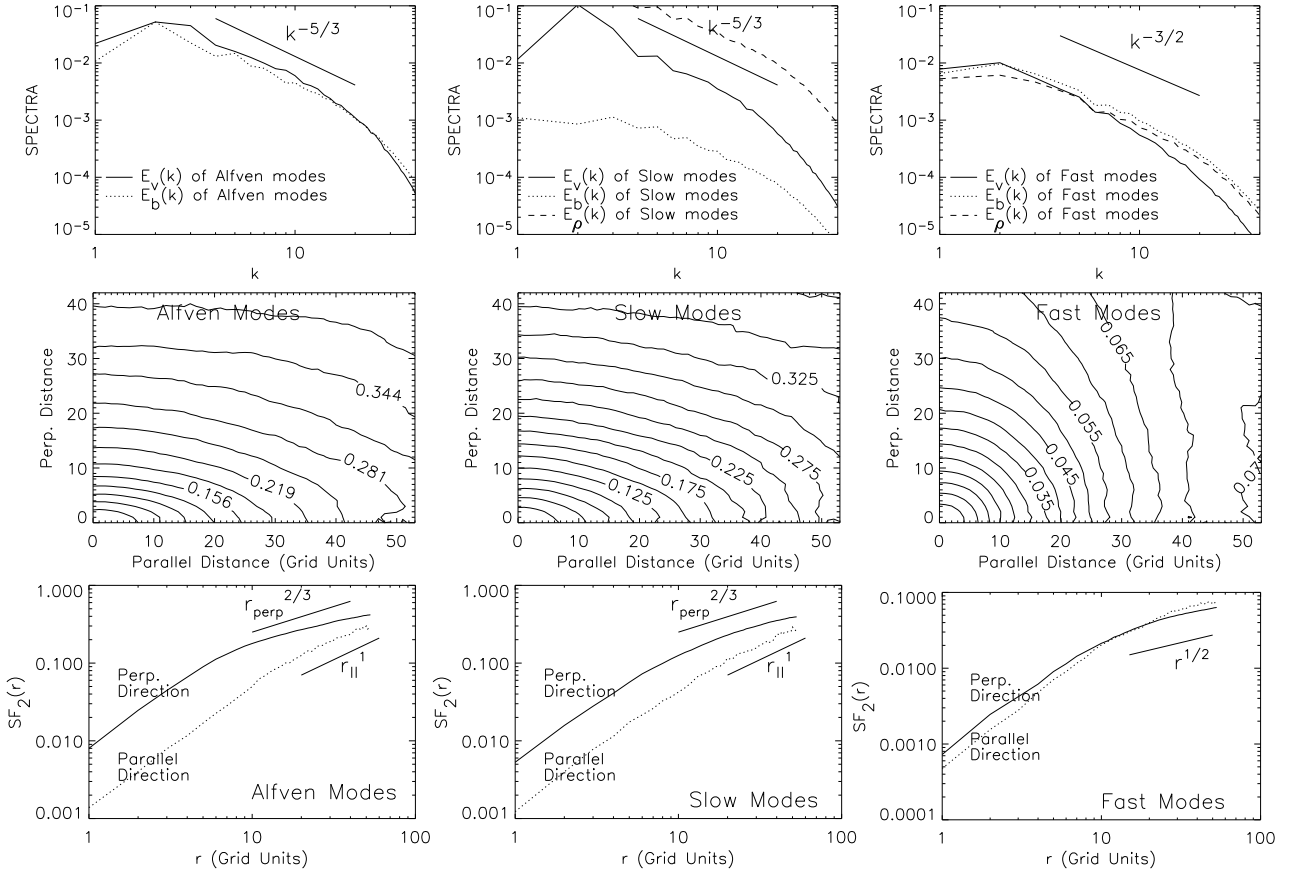


Figure 3. Low β ($\beta \sim 0.2$ and $M_s \sim 2.3$). Scalings relations. Results from driven turbulence with M_A (Alfvén Mach number) ~ 0.7 , and 216^3 grid points. ($V_A \equiv B_0/\sqrt{4\pi\rho} = 1$; a (sound speed) = $\sqrt{0.1}$; $\delta V \sim 0.7$.) (a) *Upper-left*: Spectra of Alfvén modes follow a Kolmogorov-like power law. (b) *Middle-left*: The second-order structure function (SF_2) for velocity of Alfvén modes shows anisotropy similar to the GS95 ($r_{||} \propto r_{\perp}^{2/3}$ or $k_{||} \propto k_{\perp}^{2/3}$). The structure functions are measured in directions perpendicular or parallel to the local mean magnetic field in real space. We obtain real-space velocity and magnetic fields by inverse Fourier transform of the projected fields. (c) *Lower-left*: SF_2 on the parallel axis and on perpendicular axis for Alfvén modes velocity. (d) *Upper-middle*: Spectra of slow modes also follow a Kolmogorov-like power law. (e) *Middle-middle*: Slow mode velocity shows anisotropy similar to the GS95. (f) *Lower-middle*: SF_2 on the parallel axis and on perpendicular axis for slow modes velocity. (g) *Upper-right*: Spectra of fast modes are compatible with the IK spectrum. (h) *Upper-middle*: The SF_2 of fast modes velocity shows isotropy. Fast mode magnetic field also shows isotropy. (i) *Lower-right*: SF_2 on the parallel axis and on perpendicular axis for fast modes velocity.

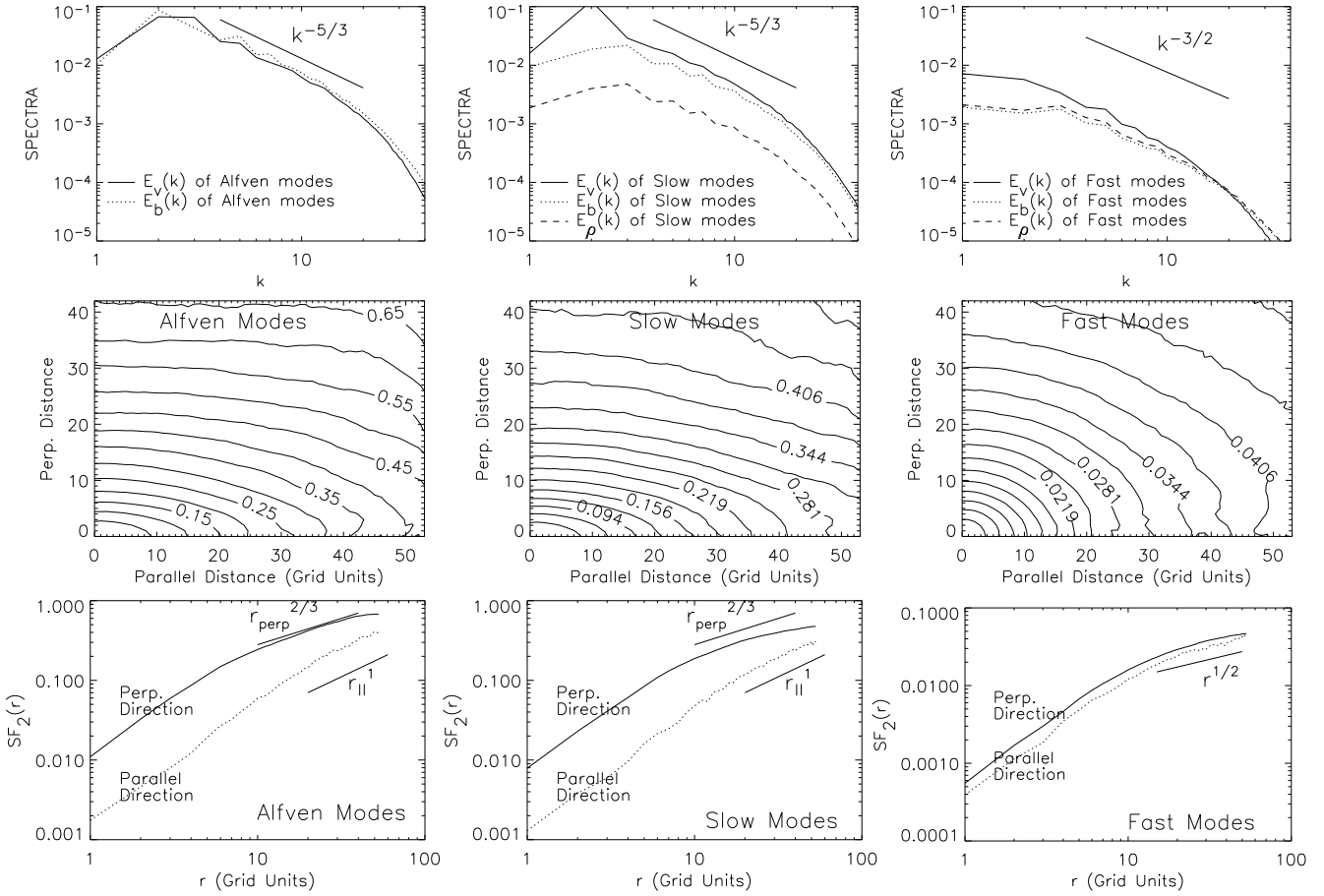


Figure 4. High β ($\beta \sim 4$ and $M_s \sim 0.35$). $V_A \equiv B_0/\sqrt{4\pi\rho} = 1$. a (sound speed) $= \sqrt{2}$. $\delta V \sim 0.7$. See caption in Fig. 3. Alfvén and slow modes follow the GS95 scalings. Fast modes are isotropic.

3 VELOCITY SCALINGS

3.1 Mode coupling

In CL02 we demonstrated the decoupling of Alfvén and fast modes in low β plasmas. Here we substantially extend the CL02 analysis. As mentioned above, the coupling of compressible and incompressible modes is crucial. If Alfvénic modes produce a copious amount of compressible motions, the whole picture of independent Alfvénic turbulence fails. However, our calculations show that the amount of energy drained into compressible motions is negligible, provided that either the external magnetic field or the gas pressure is sufficiently high. Fig. 2a suggests that the generation of compressible motions follows equation (1). Fast modes also follow a similar scaling, although the scatter is a bit larger. The marginal generation of compressible modes is in agreement with earlier studies by Boldyrev et al. (2002b) and Porter, Pouquet, & Woodward (2002), where the velocity was decomposed into a potential component and a solenoidal component. See Fig. 2a for the values of $\sim \chi$ (=the ratio of the mean square potential to solenoidal velocity). Fig. 2b demonstrates that fast modes are initially generated anisotropically, which supports our theoretical consideration in §2.1.

Fig. 2c shows that dynamics of Alfvén modes is not affected by slow modes. We first perform a driven turbulence

simulation with 216^3 grid point, $\beta \sim 0.02$, and $M_s \sim 7$. Then, after it has reached a statistically stationary state, we stop the run and save the data. Using these data, we perform two decay simulations. For one (the solid line), we remove all slow and fast modes and let the turbulence decay. For the other (the dotted line), *without* removing any modes, we just let the turbulence decay. The solid line in the figure is the energy in Alfvén modes when we start the decay simulation with Alfvén modes only. The dotted line is the Alfvén energy when we start the simulation with all modes. This result confirms that Alfvén modes cascade is almost independent of slow and fast modes. In this sense, coupling between Alfvén and other modes is weak.

3.2 High- β and mildly supersonic low- β regimes

Alfvén Modes.— Fig. 3a (low- β) and Fig. 4a (high- β) show that the power spectra of Alfvén waves follow a Kolmogorov spectrum:

$$\text{Spectrum of Alfvén Waves: } E^A(k) \propto k_{\perp}^{-5/3}. \quad (10)$$

In Fig. 3b (*middle-left panel*) and Fig. 4b (*middle-left panel*), we plot contours of equal second-order structure function for velocity ($SF_2(\mathbf{r}) = \langle |\mathbf{v}(\mathbf{x} + \mathbf{r}) - \mathbf{v}(\mathbf{x})|^2 \rangle_{\text{avg. over } \mathbf{x}}$) obtained in local coordinate systems in which the parallel axis is aligned with the local mean field (see Cho & Vishniac

2000b; CLV02a; Maron & Goldreich 2001). The SF_2 along the axis perpendicular to the local mean magnetic field follows a scaling compatible with $r^2/3$. The SF_2 along the axis parallel to the local mean field follows steeper r^1 scaling (Fig. 3c and Fig. 4c: *lower-left* panels). The results show reasonable agreement with the GS95 model for incompressible MHD turbulence,

$$\text{Anisotropy of Alfvén Waves: } r_{\parallel} \propto r_{\perp}^{2/3}, \text{ or } k_{\parallel} \propto k_{\perp}^{2/3}, \quad (11)$$

where r_{\parallel} and r_{\perp} are the semi-major axis and semi-minor axis of eddies, respectively (Cho & Vishniac 2000b).

Slow waves.— The incompressible limit of slow waves is pseudo-Alfvén waves. Goldreich & Sridhar (1997) argued that the pseudo-Alfvén waves are slaved to the shear-Alfvén (i.e. ordinary Alfvén) waves, which means that pseudo-Alfvén modes do not cascade energy for themselves. Lithwick & Goldreich (2001) made similar theoretical arguments for high β plasmas and conjectured similar behaviors of slow modes in low β plasmas. We confirmed that similar arguments are also applicable to slow waves in low β plasmas (CL02). Indeed, power spectra in Fig. 3d and Fig. 4d (*upper-middle* panels) are consistent with:

$$\text{Spectrum of Slow Modes: } E^s(k) \propto k_{\perp}^{-5/3}. \quad (12)$$

In Fig. 3e and Fig. 4e (*middle-middle* panels), contours of equal second-order velocity structure function (SF_2), representing eddy shapes, show scale-dependent anisotropy: smaller eddies are more elongated. The results show reasonable agreement with the GS95-type anisotropy

$$\text{Anisotropy of Slow Modes: } k_{\parallel} \propto k_{\perp}^{2/3}, \text{ or } r_{\parallel} \propto r_{\perp}^{2/3}, \quad (13)$$

where r_{\parallel} and r_{\perp} are the semi-major axis and semi-minor axis of eddies, respectively.

Fast waves.— Fig. 3h and Fig. 4h (*middle-right* panels) show fast modes are isotropic. The resonance conditions for the interacting fast waves are $\omega_1 + \omega_2 = \omega_3$ and $\mathbf{k}_1 + \mathbf{k}_2 = \mathbf{k}_3$. Since $\omega \propto k$ for the fast modes, the resonance conditions can be met only when all three \mathbf{k} vectors are collinear. This means that the direction of energy cascade is *radial* in Fourier space. This is very similar to acoustic turbulence, turbulence caused by interacting sound waves (Zakharov 1967; Zakharov & Sagdeev 1970; L’vov, L’vov, & Pomyalov 2000). Zakharov & Sagdeev (1970) found $E(k) \propto k^{-3/2}$. However, there is debate about the exact scaling of acoustic turbulence. Here we cautiously claim that our numerical results are compatible with the Zakharov & Sagdeev scaling:

$$\text{Spectrum of Fast Modes: } E^f(k) \sim k^{-3/2}. \quad (14)$$

The eddies are isotropic (see also Appendix B).

3.3 Highly supersonic low- β case

The results for low- β in the previous subsection are for a Mach number of ~ 2.3 . In this subsection, we present results for a Mach number of ~ 7 . Obviously shock formation is faster when the Mach number of the system is high. We also expect that turbulent motions can compress/disperse the gas more easily when the Mach number is high. As a result, we expect higher density fluctuations when Mach number is

higher. Thus we check the scaling relations for high Mach number fluids.

Fig. 5 shows that most of the scaling relations that hold true in mildly supersonic flows are still valid in the highly supersonic case. Especially anisotropy of Alfvén, slow, and fast modes is almost identical to the one in the previous section. However, the power spectra for slow modes do not show the Kolmogorov slope. The slope is close to -2 , which is suggestive of shock formation. At this moment, it is not clear whether or not the -2 slope is the true slope. In other words, the observed -2 slope might be due to the limited numerical resolution. Runs with higher numerical resolution should give the definite answer.

3.4 SuperAlfvénic turbulence

So far we considered “sub-Alfvénic” turbulence in which the Alfvén speed associated with the mean magnetic field is slightly faster than the r.m.s. fluid velocity. If the opposite case is true (i.e. if the mean field B_0 is weak), the turbulence is called “super-Alfvénic”. In super-Alfvénic turbulence, large scale magnetic field lines can show very chaotic structures. Whether or not the ISM turbulence is sub-Alfvénic is still a controversial issue.

We mentioned in §2.1 that, even in the case of super-Alfvénic turbulence, we can find some scale l' in the turbulent cascade where $v_l \sim B/\sqrt{4\pi\rho}$ and we can apply our model of sub-Alfvénic turbulence for all smaller scales. Fig. 6 supports this idea. The contours in the figure are the second order structure functions (SF_2) of velocity and magnetic field. We do not use mode decomposition. Nevertheless, the velocity SF_2 reflects scalings of Alfvén and slow modes, because fast modes are weaker than Alfvén and slow modes. As expected, anisotropy emerges at small scales. This is very similar to incompressible case (Cho & Vishniac 2000a).

Fig. 6(a) shows power spectra. We notice that the power spectra of velocity and magnetic field have different shapes. The velocity power spectrum is larger than the magnetic one near the energy injection scale at $k \sim 2.5$. However, for larger k 's ($k > 6$), the magnetic power spectrum is larger than the velocity one. This behavior is well known in incompressible simulations with unit magnetic Prandtl number (see, for example, Kida, Yanase, & Mizushima 1991; Cho & Vishniac 2000a). A similar behavior is also observed in earlier compressible simulations (see, for example, Brandenburg et al. 1996). Cho & Vishniac (2000a) argued that the transition from $E_v(k) > E_b(k)$ to $E_v(k) < E_b(k)$ occurs at a wavelength 2 or 3 time larger than that of the energy injection scale.

A careful look at Fig. 6(a) reveals that, for $k < 8$, the power spectrum of velocity declines faster than Kolmogorov as k increases. This is not very surprising because magnetic field has more power than velocity at large k 's and, therefore, can affect the velocity power spectrum at small k 's. Kida et al. (1991) claimed that the sum of $E_v(k) + E_b(k)$ roughly follows Kolmogorov spectrum in their incompressible simulations. If this is true, then the velocity power spectrum should have a spectrum steeper than Kolmogorov at small k 's because many simulations have shown that the magnetic power spectrum is significantly flatter than the velocity one at small k 's when the mean field B_0 is weak (Kida et al.

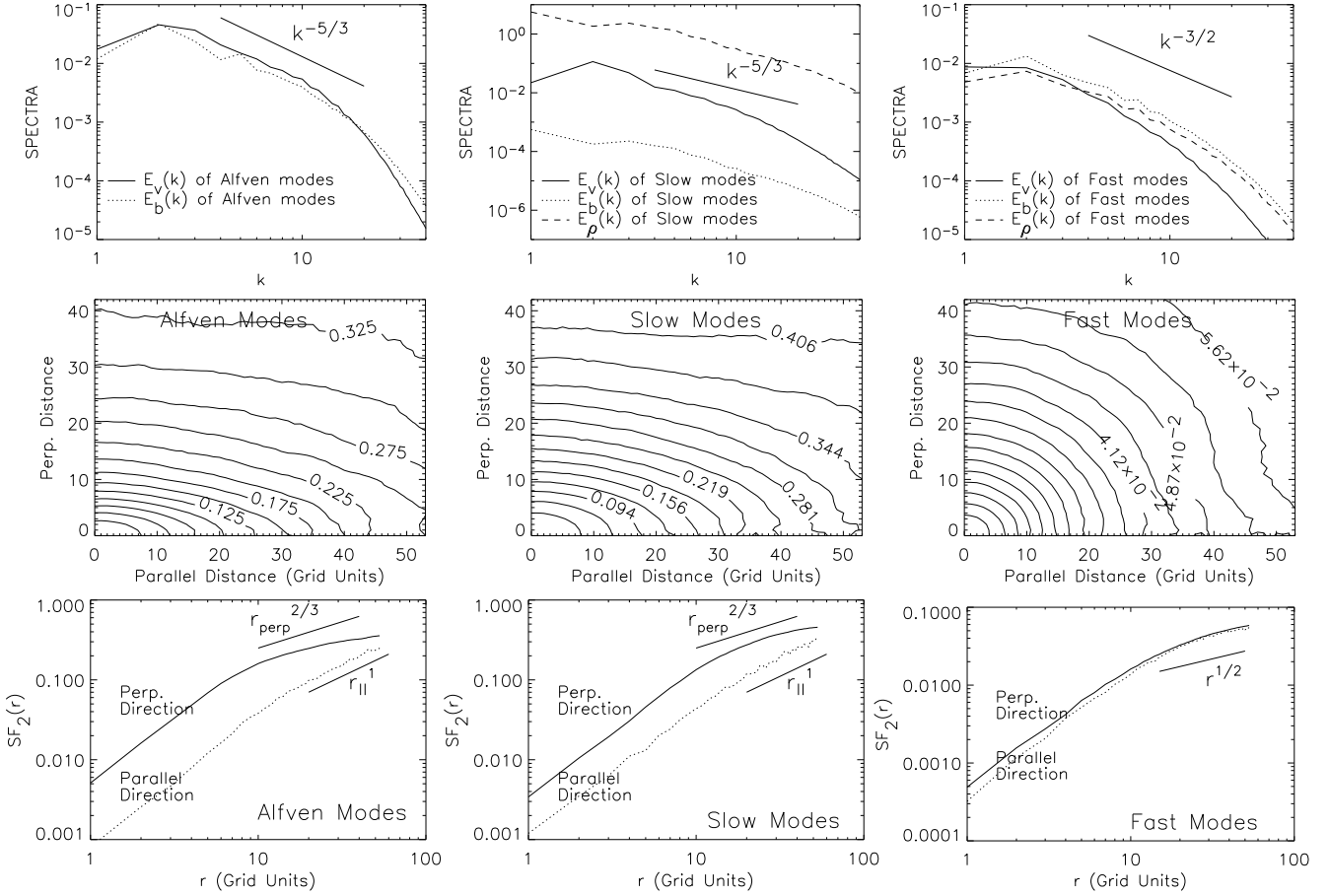


Figure 5. Highly supersonic low β ($\beta \sim 0.02$ and $M_s \sim 7$). $V_A \equiv B_0/\sqrt{4\pi\rho} = 1$. a (sound speed) = 0.1. $\delta V \sim 0.7$. Alfvén modes follow the GS95 scalings. Slow modes follow the GS95 anisotropy. But velocity spectrum of slow modes is uncertain. Fast modes are isotropic.

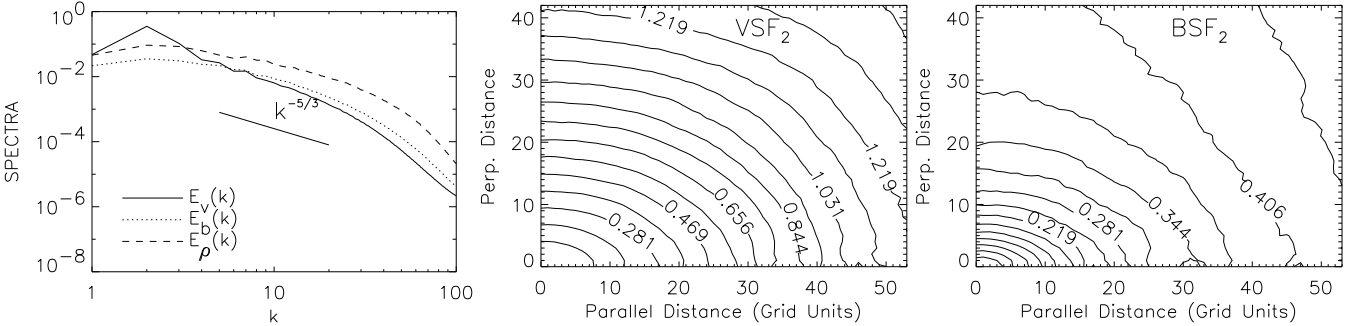


Figure 6. Super-Alfvénic turbulence ($M_A \sim 8$ and $M_s \sim 2.5$). $V_A \equiv B_0/\sqrt{4\pi\rho} = 0.1$. a (sound speed) = $\sqrt{0.1}$. $\delta V \sim 0.8$. (a)left: Spectra. (b)middle: VSF_2 . (c)right: BSF_2 . No mode decomposition is used for (b) and (c).

1991; Brandenburg et al. 1996; Cho & Vishniac 2000a). After $k \sim 8$, it seems that the velocity power spectrum gets flatter.

Boldyrev, Nordlund, & Padoan (2002a) also obtained velocity power spectrum steeper than Kolmogorov in their supersonic super-Alfvénic MHD simulations. They attributed the steep spectrum to different intermittency properties compared to the incompressible case. Since they used a different simulation set-up, we do not directly compare our results and theirs. For example, their turbulence is driven at

larger scales than ours and their sonic Mach number is larger than ours. Further parameter study is absolutely necessary.

3.5 How good is our technique?

The technique described in §2.3 is statistical in nature. That is, we separate each MHD mode with respect to the *mean* magnetic field \mathbf{B}_0 . This procedure is affected by the wan-

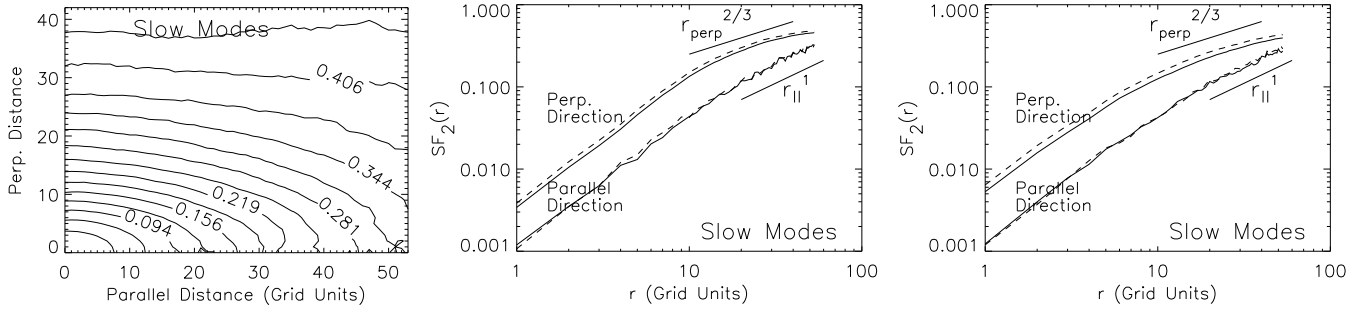


Figure 7. Comparison between Fourier space method and real space method. (a)left: From real space calculation. $M_s \sim 7$. (b)middle: Solid: Fourier space. Dashed: real space. $M_s \sim 7$. (c)right: Similar plot for $M_s \sim 2.3$.

dering of large scale magnetic field lines, as well as density inhomogeneities⁷.

Nevertheless, we can show that our technique gives statistically correct results. In low β regime, the velocity of a slow mode is nearly parallel to the *local* mean magnetic field. Therefore, for low β plasmas, we can obtain velocity statistics for slow modes in real space as follows. First, we identify the direction of the *local* mean magnetic field using the method described in Cho & Vishniac (2000b). Second, we calculate the second order structure function for slow modes by the formula $vSF_2(\mathbf{r}) = \langle |(\mathbf{v}(\mathbf{x} + \mathbf{r}) - \mathbf{v}(\mathbf{x})) \cdot \hat{\mathbf{B}}_i|^2 \rangle$, where $\hat{\mathbf{B}}_i$ is the unit vector along the *local* mean field.

Fig. 7(a) shows the contours obtained by the method for the high Mach number run. In Fig. 7(b), we compare the result obtained this way (dashed lines) and our technique described in §2.3 (solid lines). We also show a similar plot for the mildly supersonic case in Fig. 7(c). These results confirm that the method described in §2.3 gives statistically correct scaling relations.

4 LINEAR ESTIMATES OF DENSITY AND MAGNETIC FIELD FLUCTUATIONS

In this section, we estimate the magnitude of the r.m.s. fluctuations of magnetic field and density. Figures 3, 4, and 5 show that magnetic field and density have spectral indexes similar to those of velocity. We also expect that isotropy/anisotropy of magnetic field is similar to that of velocity. Therefore, we do not discuss these quantities here. However, anisotropy of density shows different behavior. Fig. 8 shows structure of density. Density shows anisotropy for the high β case. But, for low β cases, density shows more or less isotropic structures. We suspect that shock formation is responsible for the isotropization of density.

To estimate the r.m.s. fluctuations, we use the following linearized continuity and induction equations:

$$|\rho_k| = (\rho_0 v_k / c) |\hat{\mathbf{k}} \cdot \hat{\xi}|, \quad (15)$$

$$|b_k| = (B_0 v_k / c) |\hat{\mathbf{B}}_0 \times \hat{\xi}|, \quad (16)$$

⁷ One way to remove the effect by the wandering of field lines is to drive turbulence anisotropically in such a way as $k_{\perp,L} \delta V \sim k_{\parallel,L} V_A$, where $k_{\perp,L}$ and $k_{\parallel,L}$ stand for the wavenumbers of the driving scale and δV is the r.m.s. velocity. By increasing the $k_{\perp,L}/k_{\parallel,L}$ ratio, we can reduce the degree of mixing of different wave modes.

where c denotes propagation speed of slow or fast wave (equation (A22)). From this, we obtain the r.m.s. fluctuations

$$(\delta\rho/\rho_0)_s = (\delta V)_s \langle |\hat{\mathbf{k}} \cdot \hat{\xi}_s / c_s| \rangle, \quad (17)$$

$$(\delta\rho/\rho_0)_f = (\delta V)_f \langle |\hat{\mathbf{k}} \cdot \hat{\xi}_f / c_f| \rangle, \quad (18)$$

$$(\delta B/B_0)_s = (\delta V)_s \langle |\hat{\mathbf{B}}_0 \times \hat{\xi}_s / c_s| \rangle, \quad (19)$$

$$(\delta B/B_0)_f = (\delta V)_f \langle |\hat{\mathbf{B}}_0 \times \hat{\xi}_f / c_f| \rangle, \quad (20)$$

where angled brackets denote a proper Fourier space average. Generation of slow and fast modes velocity ($(\delta V)_s$ and $(\delta V)_f$) depends on driving force. Therefore, we may simply assume that

$$(\delta V)_A \sim (\delta V)_s \sim (\delta V)_f, \quad (21)$$

where we ignore constants of order unity. However, when we consider mostly incompressible driving, the generation of fast modes follows equation (1). In this case, the amplitude of fast mode velocity is reduced by a factor of

$$\left[\frac{V_A^2 + a^2}{(\delta V)_A^2} \frac{(\delta V)_A}{V_A} \right]^{-1/2} : \quad (\delta V)_A \sim (\delta V)_s \sim \left[\frac{V_A^2 + a^2}{(\delta V)_A^2} \frac{(\delta V)_A}{V_A} \right]^{1/2} (\delta V)_f. \quad (22)$$

When we assume $(\delta V)_A \sim V_A$, equation (22) reduces to equation (21) in low β plasmas.

4.1 Low- β case

In this limit, $c_s \sim a \cos \theta$ and $c_f \sim V_A$. Using equations (A31) and (A32), we obtain

$$(\delta\rho/\rho_0)_s \sim (\delta V)_s \langle |\cos \theta / c_s| \rangle \sim (\delta V)_s / a, \quad (23)$$

$$(\delta\rho/\rho_0)_f = (\delta V)_f \langle |\sin \theta / c_f| \rangle \sim (\delta V)_f / V_A, \quad (24)$$

$$(\delta B/B_0)_s = (\delta V)_s \langle |\alpha \cos \theta \sin \theta / c_s| \rangle \sim \alpha (\delta V)_s / a, \quad (25)$$

$$(\delta B/B_0)_f = (\delta V)_f \langle |1 / c_f| \rangle \sim (\delta V)_f / V_A, \quad (26)$$

where we ignore $\cos \theta$'s or $\sin \theta$'s.

When we assume $(\delta V)_A \sim (\delta V)_s \sim (\delta V)_f \sim V_A$, we get

$$(\delta\rho/\rho_0)_s \sim M_s, \quad (27)$$

$$(\delta\rho/\rho_0)_f = \sqrt{\beta} M_s, \quad (28)$$

$$(\delta B/B_0)_s = \beta M_s, \quad (29)$$

$$(\delta B/B_0)_f = \sqrt{\beta} M_s \quad (30)$$

Therefore, in low β plasmas, slow modes give rise to most of density fluctuations (CL02). On the other hand, magnetic

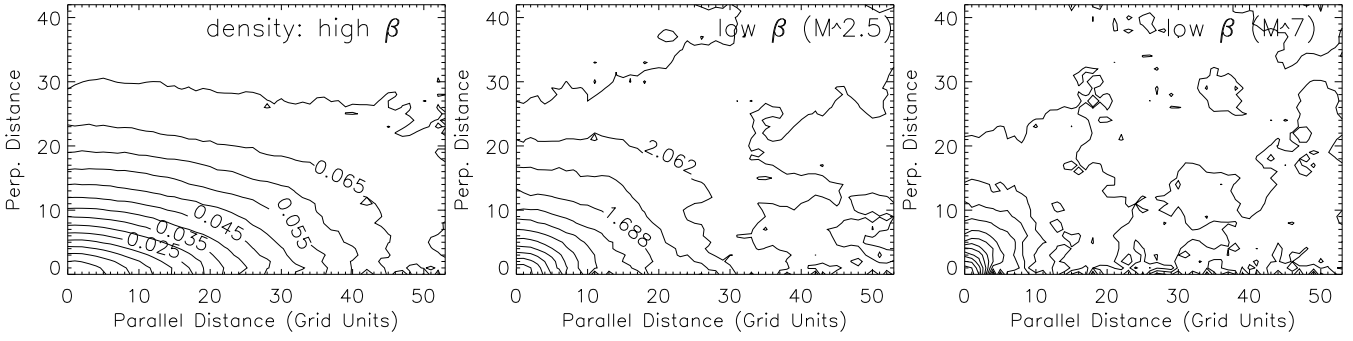


Figure 8. Density structures. (a)left: $M_s \sim 0.35$ (high β). (b)middle: $M_s \sim 2.3$ (mildly supersonic low β). (c)right: $M_s \sim 7$ (highly supersonic low β).

fluctuation by slow modes is smaller than that by fast modes by a factor of $\sqrt{\beta}$.

4.2 High- β case

In this limit, $c_s \sim V_A \cos \theta$ and $c_f \sim a$. Using equations (A33) and (A34), we obtain

$$\begin{aligned} (\delta\rho/\rho_0)_s &\sim (\delta V)_s \langle |\cos \theta \sin \theta / (a c_s)| \rangle \\ &\sim (V_A/a) (\delta V)_s / a, \end{aligned} \quad (31)$$

$$(\delta\rho/\rho_0)_f = (\delta V)_f \langle |1/c_f| \rangle \sim (\delta V)_f / a, \quad (32)$$

$$(\delta B/B_0)_s = (\delta V)_s \langle |\cos \theta / c_s| \rangle \sim (\delta V)_s / V_A, \quad (33)$$

$$(\delta B/B_0)_f = (\delta V)_f \langle |\sin \theta / c_f| \rangle \sim (\delta V)_f / a, \quad (34)$$

where we ignore $\cos \theta$'s or $\sin \theta$'s.

Let us just assume that $(\delta V)_A \sim (\delta V)_s \sim V_A \sim M_s^{-1} (\delta V)_f$ (cf. equation (22)). Then we have

$$(\delta\rho/\rho_0)_s \sim M_s / \sqrt{\beta} \sim M_s^2, \quad (35)$$

$$(\delta\rho/\rho_0)_f \sim M_s^2, \quad (36)$$

$$(\delta B/B_0)_s = O(1), \quad (37)$$

$$(\delta B/B_0)_f = M_s^2. \quad (38)$$

The density fluctuation associated with slow modes is $\sim M_s^2$, when $(\delta V)_s \sim (\delta V)_A \sim V_A$. This is consistent with Zank & Matthaeus (1993). The ratio of $(\delta\rho)_s$ to $(\delta\rho)_f$ is of order unity. Therefore, both slow and fast modes give rise to similar amount of density fluctuations. Note that this argument is of order-of-magnitude in nature. In fact, in our simulations for the high β case, the r.m.s. density fluctuation by slow modes is about twice as large as that by fast modes. When we use equation (21), we have a different result: $(\delta\rho)_s \sim (V_A/a) (\delta\rho)_f < (\delta\rho)_f$. It is obvious that slow modes dominate magnetic fluctuations: $(\delta B)_s > (\delta B)_f$ for both equations (21) and (22).

5 VISCOSITY-DAMPED REGIME OF MHD TURBULENCE

In hydrodynamic turbulence viscosity sets a minimal scale for motion, with an exponential suppression of motion on smaller scales. Below the viscous cutoff the kinetic energy contained in a wavenumber band is dissipated at that scale, instead of being transferred to smaller scales. This means

the end of the hydrodynamic cascade, but in MHD turbulence this is not the end of magnetic structure evolution. For viscosity much larger than resistivity, $\nu \gg \eta$, there will be a broad range of scales where viscosity is important but resistivity is not. On these scales magnetic field structures will be created by the shear from non-damped turbulent motions, which amounts essentially to the shear from the smallest undamped scales. The created magnetic structures would evolve through generating small scale motions. As a result, we expect a power-law tail in the magnetic energy distribution, rather than an exponential cut-off. Cho, Lazarian, & Vishniac (CLV02b) performed numerical simulations of turbulence in this regime threaded by a strong ($B_0/\sqrt{4\pi\rho} \sim \delta V$) mean magnetic field and reported that this regime possesses completely different scaling relations and anisotropic structures compared with ordinary MHD turbulence. Further research showed that there is a smooth connection between this regime and small scale turbulent dynamo in high magnetic Prandtl number fluids (see Schekochihin et al. 2002)⁸.

In partially ionized gas neutrals produce viscous damping of turbulent motions. In the Cold Neutral Medium (see Draine & Lazarian 1999 for a list of the idealized phases) this produces damping on the scale of a fraction of a parsec. The magnetic diffusion in those circumstances is still negligible and exerts an influence only at the much smaller scales, $\sim 100\text{km}$. Therefore, there is a large range of scales where the physics of the turbulent cascade is very different from the conventional MHD turbulence picture.

CLV02b explored this regime numerically with a grid of 384^3 and a physical viscosity for velocity damping. The kinetic Reynolds number was around 100. We achieved a very small magnetic diffusivity by the use of hyper-diffusion. The result is presented in Fig. 9a. A theoretical model for this regime and its consequences for stochastic reconnection (Lazarian & Vishniac 1999) can be found in Lazarian, Vishniac, & Cho (2003). It explains the spectrum $E(k) \sim k^{-1}$ as

⁸ It is worth noting that, motivated by the analogy between time evolution equations for magnetic field and for vorticity, Batchelor (1950) first argued that small magnetic fields can be amplified when viscosity is larger than magnetic diffusion (i.e. magnetic Prandtl number > 1). Although the analogy was later proved to be physically wrong, the high magnetic Prandtl number dynamo has been studied by many researchers (e.g. Kulsrud & Anderson 1992; Kinney et al. 2000).

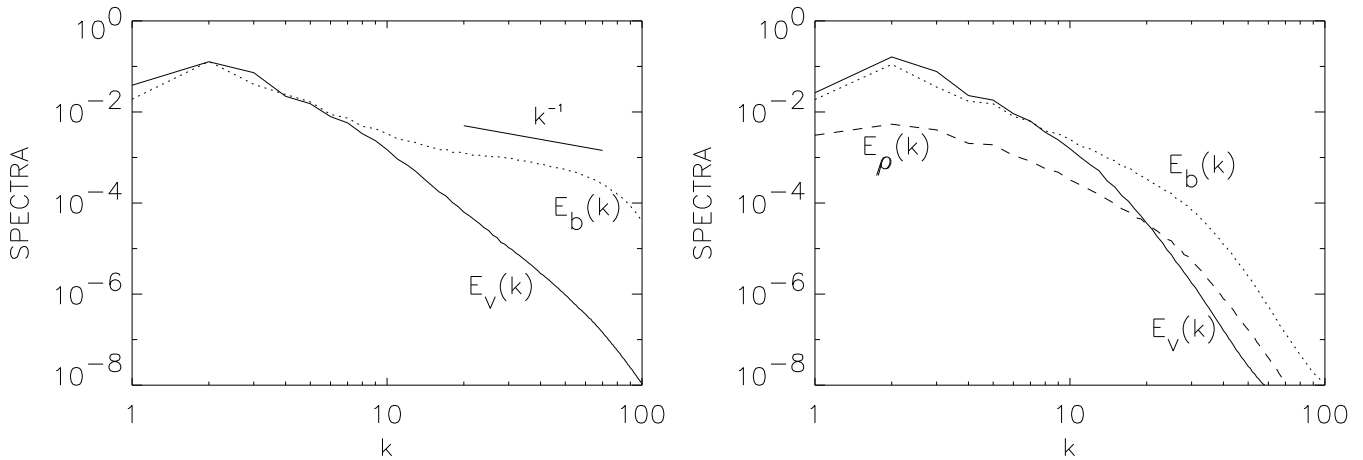


Figure 9. Viscous damped regime (viscosity > magnetic diffusivity). Due to large viscosity, velocity damps after $k \sim 10$. (a) *Left:* Incompressible case with 384^3 grid points. Magnetic spectra show a shallower slope ($E_b(k) \propto k^{-1}$) below the velocity damping scale. We achieve a very small magnetic diffusivity through the use hyper-diffusion. From Cho, Lazarian, & Vishniac (2002b). (b) *Right:* Compressible case with 216^3 grid points. Magnetic and density spectra show structures below the velocity damping scale at $k \sim 10$. The structures are less obvious than the incompressible case because it is relatively hard to achieve very small magnetic diffusivity in the compressible run.

a cascade of magnetic energy to small scales under the influence of shear at the marginally damped scales. The spectrum is similar to that of the viscous-convective range of passive scalar in hydrodynamic turbulence (see, for example, Batchelor 1959; Lesieur 1990), although the study in Lazarian, Vishniac, & Cho (2003) suggests that the physical origin of it is different. A study confirming that the k^{-1} spectrum is not a bottleneck effect is presented in Cho, Lazarian, & Vishniac (2003b). The mechanism is based on the solenoidal motions and therefore the compressibility should not alter the physics of this regime of turbulence.

We show our results for the compressible fluid in Fig 9b. We use the same physical viscosity as in incompressible case (see CLV02b). We rely on numerical diffusion, which is much smaller than physical viscosity, for magnetic field. The inertial range is much smaller due to numerical reasons, but it is clear that the viscosity-damped regime of MHD turbulence persists. The magnetic fluctuations, however, compress the gas and thus cause fluctuations in density. This is a new (although expected) phenomenon compared to our earlier incompressible calculations. These density fluctuations may have important consequences for the small scale structure of the ISM.

6 ASTROPHYSICAL IMPLICATIONS OF OUR RESULTS

6.1 Parameter range explored

Parameters of astrophysical plasmas differ substantially for different astrophysical systems: from extremely high β to extremely low β . Turbulence in some systems is expected to be superAlfvénic, in others it is expected to be subAlfvénic. Moreover, there is an ongoing controversy on what to expect and where. For instance, while high β was considered a default for many phases of Milky Way ISM, recent observations by Beck (2002) suggest that the plasmas there may be

low β . Therefore it is essential to have clear understanding of MHD turbulence for as large parameter space as possible.

SuperAlfvénic regime.— We have argued above that the difference between superAlfvénic and subAlfvénic turbulence is not as substantial as it is frequently thought. The difference between the two regimes stems from ratio of magnetic field to kinetic energies. However, as we mentioned in §2, if kinetic energy density exceed magnetic field energy density, the hydromagnetic motions drive turbulent dynamo. This enhances magnetic field energy density up to approximately equipartition value. Thus the difference between the superAlfvénic and subAlfvénic regimes amounts not to the energy of the magnetic field, but to the global level of field organization, e.g. to the magnetic field reversals etc. Our results in §3.4 suggest that the basic properties of the MHD turbulence in the subAlfvénic and superAlfvénic regimes are similar. This, however, does not preclude the intermittency of MHD turbulence being very different. The latter property can be tested using scalings of the higher order velocity correlations $SF_p(\mathbf{r}) \equiv \langle |\mathbf{v}(\mathbf{x} + \mathbf{r}) - \mathbf{v}(\mathbf{x})|^p \rangle \propto r^{\zeta(p)}$. The corresponding scaling suggested by She-Leveque (1994) contains three parameters (see Politano & Pouquet 1995; Müller & Biskamp 2000): g is related to the scaling $\delta v_l \sim l^{1/g}$, x related to the energy cascade rate $t_l^{-1} \sim l^{-x}$, and C , the co-dimension of the dissipative structures:

$$\zeta(p) = p/g(1-x) + C(1 - (1-x/C)^{p/g}). \quad (39)$$

Müller & Biskamp (2000) proposed that 3D *incompressible* MHD turbulence for *zero mean field* has Kolmogorov g and x , while the dissipation happens in the sheet-like structures, i.e. $C = 3 - 2 = 1$. Using eq. (39) they obtained an excellent fit for their *incompressible* data. Later Boldyrev (2002) made the same assumption⁹ that $C = 1$ (and same g

⁹ The physical motivation of Müller & Biskamp (2000) and Boldyrev (2002) for choosing the same value of C are different, however. Boldyrev (2002) identifies the dissipation structures

and x) for the compressible turbulence and Boldyrev, Nordlund, & Padoan (2002a) obtained an excellent fit to their *compressible* data. It appears surprising that incompressible MHD (Müller & Biskamp 2000) and supersonic compressible MHD (Boldyrev et al. 2002a) have similar intermittency structures. This issue is discussed in Cho, Lazarian, & Vishniac (2003b).

We would like to note, however, that our considerations about superAlfvénic turbulence are not applicable to the transient regimes when superAlfvénic motions are in the process of generating magnetic field and magnetic energy does not have time to come to a rough equipartition to the kinetic energy. Some parts of the ISM can well be in the transient regime for which temporary $\rho V^2/2 \gg B^2/8\pi$.

$\beta = 1$ case.— We provided theoretical considerations for both $\beta \gg 1$ and $\beta \ll 1$ cases. What about the intermediate cases of $\beta \sim 1$? Would the scaling of modes and mode coupling be different? To test this case we performed calculations for $\beta = 1$. The results in Fig. 10 show that the scaling relations that hold true for mildly low β regime are also applicable for $\beta = 1$ regime.

6.2 Fundamental questions

How fast does MHD turbulence decay? This question has fundamental implications for *star formation* (see McKee 1999). Indeed, it was thought originally that magnetic fields would prevent turbulence from fast decay. Later (see Mac Low et al. 1998; Stone et al. 1998; and review by Vazquez-Semadeni et al. 2000) this was reported not to be true. However, fast decay was erroneously associated with the coupling between compressible and incompressible modes. The idea was that incompressible motions quickly transfer their energy to the compressible modes, which get damped fast by direct dissipation (presumably through shock formation).

Our calculations support the conjecture given by eq. (1). According to it the coupling of Alfvén and compressible motions is important only at the energy injection scales where $\delta V_i \sim V_A$. As the turbulence evolves the perturbations become smaller and the coupling less efficient. Typically for numerical simulations the inertial range is rather small and this could explain why marginal coupling of modes was not noticed.

Our results show that MHD turbulence damping does not depend on whether the fluid is compressible or not. The incompressible motions damp also within one eddy turnover time¹⁰. This is the consequence of the fact that within the strong turbulence¹¹ mixing motions perpendicular to magnetic field are hydrodynamic to high order (CLV02a) and

with shocks, which are absent in *incompressible* simulations by Müller & Biskamp (2000).

¹⁰ It is generally believed that decay of turbulence energy follows a power-law. A possible expression is $E(t) \sim E_0/[1 + C(t - t_0)]^n$ (C. McKee, private communication), where E_0 is the energy at the initial time t_0 . Our claim is that decay of turbulence follows $E(t) \sim E_0/[1 + C'(t - t_0)/t_{cas,0}]^n$, where $t_{cas,0}$ is the eddy turnover time at $t = t_0$ and C' is a constant of order unity.

¹¹ For a formal definition of strong, weak and intermediate turbulence, see Goldreich & Sridhar (1997) and CLV03a, but here we just mention in passing that in most astrophysically important cases the MHD turbulence is “strong”.

the cascade of energy induced by those motions is similar to the hydrodynamic one, i.e. energy cascade happens within an eddy turnover time.

The reported (see Mac Low et al. 1998) decay of the *total* energy of turbulent motions E_{tot} follows t^{-1} which can be understood if we account for the fact that the energy is being injected at the scale smaller than the scale of the system. Therefore some energy originally diffuses to larger scales through the inverse cascade. Our calculations stimulated by illuminating discussions with Chris McKee show that if this energy transfer is artificially prevented by injecting the energy on the scale of the computational box, the scaling of E_{tot} becomes closer to t^{-2} .

Can compressible MHD turbulence decay slowly? Incompressible MHD computations (see Maron & Goldreich 2001; CLV02a) show that the rate of turbulence decay depends on the degree of turbulence imbalance¹², i.e. the difference in the energy fluxes moving in opposite directions. The strongly imbalanced incompressible turbulence was shown to persist longer than its balanced counterpart. This enabled CLV02a to speculate that this may enable energy transfer between clouds and may explain the observed turbulent linewidths of GMCs without evident star formation. Imbalanced turbulence can also make it possible to transfer energy from the galactic disk to heat the Reynolds layer (see Reynolds 1988).

Our results above show a marginal coupling of compressible and incompressible modes. This is suggestive that the results obtained in incompressible simulations are applicable to compressible environments if amplitudes of perturbations are not large. The complication arises from the existence of the parametric instability (Del Zanna, Velli, & Londrillo 2001) that happens as the density perturbations reflect Alfvén waves and grow in amplitude. This instability eventually controls the degree of imbalance that is achievable. However, the growth rate of the instability is substantially slower than the Alfvén wave oscillation rate. Therefore, if we take into account that interstellar sources are intermittent not only in space, but also in time, the transport of turbulent energy described in CLV02a seems feasible. Here we mention that the growth of the parametric instability described above may provide an alternative explanation for the observed infall motions of the cloud cores (Tafalla et al. 1998). Earlier those motions were explained as arising from linear damping of Alfvén waves (Myers & Lazarian 1998).

Is the correlation between magnetic field and density tight in MHD turbulence? In the traditional static paradigm of the ISM, density and magnetic field increase simultaneously as clouds contract. Introduction of turbulence in the picture of ISM complicates the analysis (see discussion in Vazquez-Semadeni et al. 2000; CLV03a). Our results confirm earlier claims (e.g. Passot & Vazquez-Semadeni 2003) that magnetic field - density correlations may be weak. First of all, some magnetic field fluctuations are related to Alfvénic turbulence which does not compress the medium. Second, slow modes in low β plasmas are essentially density perturbations that propagate along mag-

¹² This quantity is also called cross helicity (see Matthaeus, Goldstein, & Montgomery 1983).

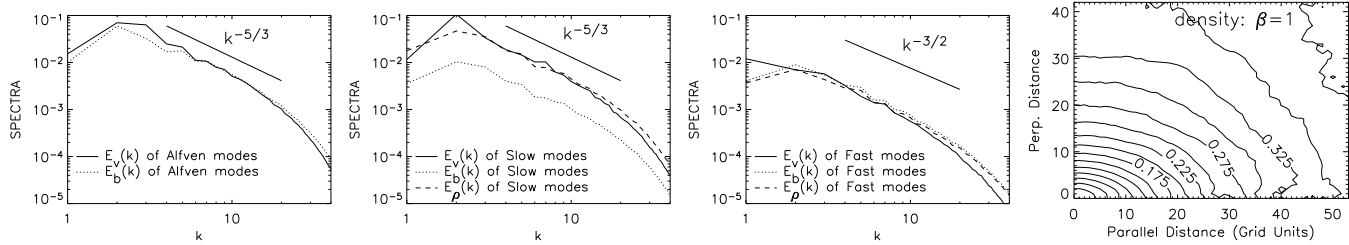


Figure 10. $\beta = 1$ case. (a)left: Alfvén mode spectra. (b)second-left: Slow mode spectra. (c)second-right: Fast mode spectra. (d)right: Density structure.

netic field and which marginally perturb magnetic fields. Moreover, our calculations (see Fig. 8) show that at substantially high Mach numbers the density correlations do not show anisotropies, while magnetic field fluctuations are anisotropic. On the basis of our calculations we might expect that the correlation may be a bit higher for high β than for low β plasmas.

Can viscously damped turbulence explain TSAS? The term “tiny-scale atomic structures” or TSAS was introduced by Heiles (1997) to describe the mysterious H I absorbing structures on scales from thousands to tens of AU, discovered by Dieter, Welch & Romney (1976). Analogs of TSAS are observed in NaI and CaII (Meyer & Blades 1996; Faison & Goss 2001; Andrews, Meyer, & Lauroesch 2001) and in molecular gas (Marscher, Moore, & Bania 1993).

Those structures can be produced by turbulence with a spectrum substantially more shallow than the Kolmogorov one, e.g. with the spectrum $E(k) \sim k^{-1}$ (see Deshpande 2000). Simulations in CLV02b and theoretical calculations in Lazarian, Vishniac & Cho (2003) show that the magnetic field in the viscosity-damped regime of MHD turbulence (see §5) can produce such a spectrum of magnetic fluctuations. Our calculations above are indicative that this will translate in the corresponding shallow spectrum of density. Our calculations are applicable on scales from the viscous damping scale (determined by equating the energy transfer rate with the viscous damping rate; ~ 0.1 pc in the Warm Neutral Medium with $n = 0.4 \text{ cm}^{-3}$, $T = 6000$ K) to the ion-neutral decoupling scale (the scale at which viscous drag on ions becomes comparable to the neutral drag; $\ll 0.1$ pc). Below the viscous scale the fluctuations of magnetic field obey the damped regime shown in Figure 9b and produce density fluctuations. For typical Cold Neutral Medium gas, the scale of neutral-ion decoupling decreases to ~ 70 AU, and is less for denser gas. TSAS may be created by strongly nonlinear MHD turbulence!

6.3 Application of the scaling laws obtained

Many astrophysical problems require some knowledge of the scaling properties of turbulence. Therefore we expect a wide range of applications of the established scaling relations. Here we discuss how our understanding of MHD turbulence affects a few selected issues.

As we mentioned in the introduction, the observations (see CLV03a for a review) indicate that interstellar spectrum exhibits Kolmogorov-type scaling $E(k) \sim k^{-5/3}$. On the basis of what we learned by now (see also Higdon 1983,

GS95, Lithwick & Goldreich 2001, CL02) we may conclude that the MHD spectrum *is different* from the spectrum of isotropic Kolmogorov turbulence. Anisotropy of Alfvénic and slow modes ensures that the observationally measured spectrum is dominated by perturbations perpendicular to the magnetic field, i.e. $E(k) \sim k_{\perp}^{-5/3}$. Admixture of fast modes can alter the spectrum, but observations indicate that those modes do not dominate the detected signal.

Whether or not one can use Kolmogorov isotropic scaling for practical calculations depends on the nature of the problem. For instance, Cho & Lazarian (2002b) use Kolmogorov scaling to calculate the spectra of fluctuations arising from synchrotron emission and of fluctuations of the degree of starlight polarization and obtained good correspondence with the observed statistics. However, for many problems turbulence anisotropy is essential.

Cosmic rays.— The propagation of cosmic rays is mainly determined by their interactions with electromagnetic fluctuations in the interstellar medium. For practical calculations it is usually assumed that the turbulence is *isotropic* with a Kolmogorov spectrum (e.g., Schlickeiser & Miller 1998). How should these calculations be modified in view of our findings? Chandran (2000) and Yan & Lazarian (2002; see also Lazarian, Cho & Yan 2002 for a review) calculated the efficiency of cosmic ray scattering by Alfvénic modes and found that, if the energy injected at large scales, the scattering by Alfvénic modes is absolutely negligible. The difference between the calculations in Yan & Lazarian (2002), which used the tensor description of Alfvén waves obtained in CLV02a, and the calculations that use Kolmogorov turbulence was 10 orders of magnitude! Yan & Lazarian (2002; 2003a) identified fast modes as the principal source of cosmic ray scattering and used the CL02 results to calculate the scattering rate in low β plasma. Damping of those modes, however, depends on the value of β , which entails the dependence of cosmic ray scattering on the temperature and density of the background plasmas.

Dust dynamics.— Turbulence induces relative dust grain motions and leads to grain-grain collisions. These collisions determine grain size distribution, which affects most dust properties, including absorption and H_2 formation. Unfortunately, as in the case of cosmic rays, earlier work appealed to hydrodynamic turbulence to predict grain relative velocities. Lazarian & Yan (2002) and Yan & Lazarian (2003b) considered motions of charged grains in anisotropic MHD turbulence and found that the direct interaction of the charged grains with turbulent magnetic field results in a stochastic acceleration that can potentially provide grains with supersonic velocities.

Other applications.— The obtained scaling laws are essential for understanding the density fluctuations within HII regions (Lithwick & Goldreich 2001), stochastic magnetic reconnection in fully ionized (Lazarian & Vishniac 1999, 2000) and partially ionized plasma (Lazarian, Vishniac & Cho 2003), for energy transfer to electrons in gamma ray bursts and solar flares (see Lazarian, Petrosian, Yan, & Cho 2003). This list can be easily extended.

7 SUMMARY

In the paper, we have studied statistics of compressible MHD turbulence for high, intermediate, and low β plasmas and for different sonic and Alfvén Mach numbers. For sub-Alfvénic turbulence we provided the decomposition of turbulence into Alfvén, slow and fast modes. We have found that the coupling of compressible and incompressible modes is weak and, contrary to the common belief, the drain of energy from Alfvén to compressible modes is marginal along the cascade. For the cases studied, we have found that GS95 scaling is valid for *Alfvén modes*:

$$\text{Alfvén: } E^A(k) \propto k^{-5/3}, \quad k_{\parallel} \propto k_{\perp}^{2/3}.$$

Slow modes also follows the GS95 model for both high β and mildly supersonic low β cases:

$$\text{Slow: } E^s(k) \propto k^{-5/3}, \quad k_{\parallel} \propto k_{\perp}^{2/3}.$$

For the highly supersonic low β case, the kinetic energy spectrum of slow modes tends to be steeper, which may be related to the formation of shocks.

Fast mode spectra are compatible with acoustic turbulence scaling relations:

$$\text{Fast: } E^f(k) \propto k^{-3/2}, \text{ isotropic spectrum.}$$

Our super-Alfvénic turbulence simulations suggest that the picture above holds true at sufficiently small scales at which Alfvén speed V_A is larger than the turbulent velocity v_t . This part of our study shows that compressible MHD turbulence is not a mess. On the contrary, its statistics obeys well determined universal scaling relations. The importance of these relations for different branches of Astrophysics is obvious.

Addressing the issue of MHD turbulence damping in partially ionized gas we showed that the viscosity-damped regime of MHD turbulence below the viscous damping scale that was reported in CLV02b for incompressible fluid persists when compressibility is present. The spectrum of density fluctuations that we obtain may be related to the mysterious tiny scale structures observed in the ISM.

ACKNOWLEDGMENTS

We thank Ethan Vishniac, Peter Goldreich, Bill Matthaeus, Chris McKee, and Annick Pouquet for stimulating discussions. We acknowledge the support of NSF Grant AST-0125544. This work was partially supported by NCSA under AST010011N and utilized the NCSA Origin2000.

REFERENCES

- Andrews, S. M., Meyer, D. M., & Lauroesch, J. T. 2001 ApJ, 552, L73
 Armstrong, J. W., Rickett, B. J., & Spangler, S. R. 1995, ApJ, 443, 209
 Batchelor, G. K. 1950, Proc. Roy. Soc. Lond., A201, 405
 Batchelor, G. K. 1959, J. Fluid Mech., 5, 113
 Beck, R. 2002, preprint (astro-ph/0212288)
 Bertoglio, J.-P., Bataille, F., & Marion, J.-D. 2001, Phys. Fluids, 13, 290
 Boldyrev, S. 2002, ApJ, 569, 841
 Boldyrev, S., Nordlund, Å., & Padoan P. 2002a, ApJ, 573, 678
 Boldyrev, S., Nordlund, Å., & Padoan P. 2002b, Phys. Rev. Lett. 89, 031102
 Brandenburg, A., Jennings, R., Nordlund, A., Rieutord, M., Stein, R., & Tuominen, I. 1996, J. Fluid Mech., 306, 325
 Chandran, B. 2001, Phys. Rev. Lett., 85(22), 4656
 Cho, J., Lazarian, A. 2002a, Phys. Rev. Lett., 88, 245001 (CL02)
 Cho, J., Lazarian, A. 2002b, ApJ, 575, L63
 Cho, J., Lazarian, A., & Vishniac, E. 2002a, ApJ, 564, 291 (CLV02a)
 Cho, J., Lazarian, A., & Vishniac, E. 2002b, ApJ, 566, L49 (CLV02b)
 Cho, J., Lazarian, A., Honein, A., Knaepen, B., Kassinos, S., & Moin, P. 2003, ApJ, 589, L77
 Cho, J., Lazarian, A., & Vishniac, E. 2003a, in *Turbulence and Magnetic Fields in Astrophysics*, eds. E. Falgarone & T. Passot (Springer LNP), p56 (astro-ph/0205286) (CLV03a)
 Cho, J., Lazarian, A., & Vishniac, E. 2003b, ApJ, accepted (astro-ph/0305212)
 Cho, J. & Vishniac, E. 2000b, ApJ, 539, 273
 Cho, J. & Vishniac, E. 2000a, ApJ, 538, 217
 Del Zanna, L., Velli, M., & Londrillo, P. 2001, A&A, 367, 705
 Deshpande, A. A. 2000, MNRAS, 317, 199
 Deshpande, A. A., Dwarakanath, K. S., & Goss, W. M. 2000, ApJ, 543, 227
 Dieter, N. H., Welch, W. J., & Romney, J. D. 1976, ApJ, 206, L113
 Draine, B. T. & Lazarian, A. 1999, ApJ, 512, 740
 Faison, M. D. & Goss, W. M. 2001, AJ, 121, 2706
 Goldreich, P. & Sridhar, S. 1995, ApJ, 438, 763
 Goldreich, P. & Sridhar, S. 1997, ApJ, 485, 680
 Heiles, C. 1997, ApJ, 481, 193
 Higdon, J. C. 1984, ApJ, 285, 109
 Jiang, G. & Wu, C. 1999, J. Comp. Phys., 150, 561
 Kida, S., Yanase, S., & Mizushima, J. 1991, Phys. Fluids A, 3, 457
 Kinney, R. M., Chandran, B., Cowley, S., & McWilliams, J. C. 2000, ApJ, 545, 907
 Kolmogorov, A. 1941, Dokl. Akad. Nauk SSSR, 31, 538
 Kulsrud, R. & Anderson, S. 1992, ApJ, 396, 606
 Lazarian, A., Cho, J., & Yan, H. 2002, preprint (astro-ph/0211031)
 Lazarian, A. & Esquivel, E. 2003, ApJ, accepted (astro-ph/0304007)
 Lazarian, A., Petrosian, V., Yan, H., & Cho, J. 2003, in

press (astro-ph/0301181)
 Lazarian, A. & Pogosyan, D. 2000, ApJ, 537, 720
 Lazarian, A. & Vishniac, E. T. 1999, ApJ, 517, 700
 Lazarian, A. & Vishniac, E. T. 2000, Rev. Mex. A&A, 9, 55
 Lazarian, A. & Vishniac, E. T., & Cho, J. 2003, ApJ, submitted
 Lazarian, A. & Yan, H. 2002, ApJ, 566, L105
 Leamon, R. J., Smith, C. W., Ness, N. F., Matthaeus, W. H., & Wong, H. 1998, J. Geophys. Res., 103, 4775
 Lesieur, M. 1990, Turbulence In Fluids (Dordrecht: Kluwer)
 Lithwick, Y. & Goldreich, P. 2001, ApJ, 562, 279
 Liu, X. & Osher, S. 1988, J. Comp. Phys., 141, 1
 L'vov, V. S. & L'vov, Y. V., & Pomyalov, A. 2000, Phys. Rev. E, 61, 2586
 McKee, C. F. 1999, in *The Origin of Stars and Planetary Systems*, ed. by J. L. Charles, D. K. Nikolaos (Dordrecht: Kluwer, 1999) p.29
 Mac Low, M.-M., Klessen, R., Burkert, A., & Smith, M. 1998, Phys. Rev. Lett., 80, 2754
 Maron, J. & Goldreich, P. 2001, ApJ, 554, 1175
 Marscher, A. P., Moore, E. M., & Bania, T. M. 1993, ApJ, 419, L101
 Matthaeus, W. H. & Brown, M. R. 1988, Phys. Fluids, 31(12), 3634
 Matthaeus, W. H., Ghosh, S., Oughton, S., & Roberts, D. A. 1996, J. Geophysical Res., 101(A4), 7619
 Matthaeus, W. H., Goldstein, M. L., Montgomery, D. C. 1983, Phys. Rev. Lett., 51, 1484
 Meyer, D. M. & Blades, J. C. 1996, ApJ, 464, L179
 A. S. Monin, A. A. Yaglom: *Statistical Fluid Mechanics: Mechanics of Turbulence*, Vol. 2 (Cambridge: MIT Press, 1975)
 Myers, P. & Lazarian, A. 1998m ApJ, 507, 157
 Müller, W.-C. & Biskamp, D. 2000, Phys. Rev. Lett., 84(3), 475
 Padoan, P. & Nordlund, A. 1999, ApJ, 526, 279
 Passot, T. & Vazquez-Semadeni, E. 2003, A&A, 398, 845
 Politano, H. & Pouquet, A. 1995, Phys. Rev. E, 52, 636
 Reynolds, R. J. 1988, ApJ, 333, 341
 Schekochihin, A., Maron, J., Cowley, S., & McWilliams, J. 2002, ApJ, 576, 806
 Schlickeiser, A. & Miller, J. A. 1998, ApJ, 492, 352
 She, Z. & Leveque, E. 1994, Phy. Rev. Lett. 72, 336
 Shebalin, J. V., Matthaeus, W. H., & Montgomery, D. C. 1983, J. Plasma Phys., 29, 525
 Spangler, S.R. 1991, ApJ, 376, 540
 Spangler, S.R. 1999, ApJ, 522, 879
 Stanimirovic, S. & Lazarian, A. 2001, ApJ, 551, L53
 Stone, J., Ostriker, E., & Gammie, C. 1998, ApJ, 508, L99
 Tafalla, M., Mardones, D., Myers, P., Caselli, P., Bachiller, R., & Benson, B. 1998, ApJ, 504, 900
 Thompson, W. B. 1962, *An Introduction to Plasma Physics*, (Pergamon Press)
 Vazquez-Semadeni, E. 2000, in *Advanced Series in Astrophysics and Cosmology, Vol. 10*, eds. V. Gurzadyan & R. Ruffini (World Scientific), p.379
 Vazquez-Semadeni, E., Ostriker, E.C., Passot, T., Gammie, C.F., & Stone, J.M. 2000, in *Protostars and Planets IV*, eds. V. Mannings et al. (Tucson: University of Arisona Press), p.3

Yan, H. & Lazarian, H. 2002, Phy. Rev. Lett., 89, 281102
 Yan, H. & Lazarian, H. 2003a, ApJ, accepted (astro-ph/0301007)
 Yan, H. & Lazarian, H. 2003b, ApJ, submitted
 Zakharov, V. E. 1967, Sov. Phys. JETP, 24, 455
 Zakharov, V. E. & Sagdeev, A. 1970, Sov. Phys. Dokl. 15, 439
 Zank, G. P. & Matthaeus, W. H. 1993, Phys. Fluids A, 5(1), 257

APPENDIX A: MODE DECOMPOSITION

Let us consider a small perturbation in the presence of a strong mean magnetic field. We write density, velocity, pressure, and magnetic field as the sum of constant and fluctuating parts: $\rho \rightarrow \rho_0 + \rho$, $\mathbf{v} \rightarrow \mathbf{v}_0 + \mathbf{v}$, $P \rightarrow P_0 + p$, and $\mathbf{B} \rightarrow \mathbf{B}_0 + \mathbf{b}$, respectively. We assume that $\mathbf{v}_0 = 0$ and that perturbation is small : $\rho \ll \rho_0$, etc. Ignoring the second and higher order contributions, we can rewrite the MHD equations as follows:

$$\frac{\partial \rho}{\partial t} + \rho_0 \nabla \cdot \mathbf{v} = 0, \quad (\text{A1})$$

$$\rho_0 \frac{\partial \mathbf{v}}{\partial t} + \nabla(a^2 \rho) - \frac{1}{4\pi} (\nabla \times \mathbf{b}) \times \mathbf{B}_0 = 0, \quad (\text{A2})$$

$$\frac{\partial \mathbf{b}}{\partial t} + \nabla \times [\mathbf{v} \times \mathbf{B}_0] = 0, \quad (\text{A3})$$

where we assume a polytropic equation of state: $p = a^2 \rho$ with $a^2 = \gamma p_0 / \rho_0$. We follow arguments in Thompson (1962) to derive magnetosonic waves. Let $\xi(\mathbf{r}, t)$ be the displacement vector, so that $\partial \xi / \partial t = \mathbf{v}$. Assuming that the displacements vanish at $t = 0$, we can integrate the equations as follows

$$\rho + \rho_0 \nabla \cdot \xi = 0, \quad (\text{A4})$$

$$\ddot{\xi} = a^2 \nabla (\nabla \cdot \xi) + (\nabla \times \mathbf{b}) \times \mathbf{B}_0 / 4\pi \rho_0, \quad (\text{A5})$$

$$\mathbf{b} = \nabla \times (\xi \times \mathbf{B}_0). \quad (\text{A6})$$

The momentum equation (eq. A5) becomes

$$\begin{aligned} \ddot{\xi} &= a^2 \nabla (\nabla \cdot \xi) + [\nabla \times (\nabla \times (\xi \times \mathbf{B}_0))] \times \mathbf{B}_0 / 4\pi \rho_0 \\ &= a^2 \nabla (\nabla \cdot \xi) + \nabla (B_0^2 \nabla \cdot \xi - \mathbf{B}_0 \cdot \nabla \mathbf{B}_0 \cdot \xi) / 4\pi \rho_0 \\ &\quad - (\mathbf{B}_0 \cdot \nabla)^2 \xi / 4\pi \rho_0 + [\mathbf{B}_0 (\mathbf{B}_0 \cdot \nabla) \nabla \cdot \xi] / 4\pi \rho_0 \end{aligned} \quad (\text{A7})$$

Using $\alpha = a^2 / V_A^2 = \beta(\gamma/2)$, $V_A = B_0 / 4\pi \rho_0$, we have

$$\ddot{\xi} / V_A^2 - \nabla [(\alpha + 1) \nabla \cdot \xi - (\hat{\mathbf{B}}_0 \cdot \nabla) (\hat{\mathbf{B}}_0 \cdot \xi)] - (\hat{\mathbf{B}}_0 \cdot \nabla)^2 \xi + (\hat{\mathbf{B}}_0 \cdot \nabla) (\nabla \cdot \xi) \hat{\mathbf{B}}_0 = 0 \quad (\text{A8})$$

In Fourier spacethe equation becomes

$$\ddot{\xi} / V_A^2 + k \hat{\mathbf{k}} [(\alpha + 1) k \xi_k - k_{\parallel} \xi_{\parallel}] + k_{\parallel}^2 \xi - k_{\parallel} k \xi_k \hat{k}_{\parallel} = 0, \quad (\text{A9})$$

where $\xi_k = \xi \cdot \hat{\mathbf{k}}$, $\xi_{\parallel} = \xi \cdot \hat{\mathbf{k}}_{\parallel}$, $\hat{\mathbf{k}} = \mathbf{k} / k$, and $\hat{\mathbf{k}}_{\parallel}$ is unit vector parallel to \mathbf{B}_0 (i.e. $\hat{\mathbf{k}}_{\parallel} = \hat{\mathbf{B}}_0$). Assuming $\ddot{\xi} = -\omega^2 \xi = -c^2 k^2 \xi$, we can rewrite (A9) as

$$(c^2 / V_A^2 - \cos^2 \theta) \xi - [(\alpha + 1) \xi_k - \cos \theta \xi_{\parallel}] \hat{\mathbf{k}} + \cos \theta \xi_k \hat{k}_{\parallel} = 0, \quad (\text{A10})$$

where $\cos \theta = k_{\parallel} / k$ and θ is the angle between \mathbf{k} and \mathbf{B}_0 .

Using $\hat{\mathbf{k}} = \sin \theta \hat{\mathbf{k}}_{\perp} + \cos \theta \hat{\mathbf{k}}_{\parallel}$, we get

$$\begin{aligned} (c^2 / V_A^2 - \cos^2 \theta) \xi - [(\alpha + 1) \xi_k - \cos \theta \xi_{\parallel}] \sin \theta \hat{\mathbf{k}}_{\perp} \\ - [(\alpha + 1) \xi_k - \cos \theta \xi_{\parallel}] \cos \theta - \cos \theta \xi_k \hat{k}_{\parallel} = 0. \end{aligned} \quad (\text{A11})$$

Writing $\xi = \xi_{\perp} \hat{\mathbf{k}}_{\perp} + \xi_{\parallel} \hat{\mathbf{k}}_{\parallel} + \xi_{\varphi} \hat{\varphi}$, we get

$$(c^2/V_A^2 - \cos^2 \theta) \xi_{\perp} - [(\alpha + 1)\xi_k - \cos \theta \xi_{\parallel}] \sin \theta = 0, \quad (\text{A12})$$

$$(c^2/V_A^2 - \cos^2 \theta) \xi_{\parallel} - [\alpha \xi_k - \cos \theta \xi_{\parallel}] \cos \theta = 0, \quad (\text{A13})$$

$$(c^2/V_A^2 - \cos^2 \theta) \xi_{\varphi} = 0. \quad (\text{A14})$$

The non-trivial solution of equation (A14) is the Alfvén wave, whose dispersion relation is $\omega/k = V_A \cos \theta$. The direction of the displacement vector for Alfvén wave is parallel to the azimuthal basis $\hat{\varphi}$:

$$\hat{\xi}_A = -\hat{\varphi} = \hat{\mathbf{k}}_{\perp} \times \hat{\mathbf{k}}_{\parallel}. \quad (\text{A15})$$

Let us consider solutions of equations (A12) and (A13). Using $\xi_k = \xi_{\perp} \sin \theta + \xi_{\parallel} \cos \theta$, we get

$$(c^2/V_A^2 - \cos^2 \theta) \xi_{\perp} - (\alpha + 1) \sin^2 \theta \xi_{\perp} - \alpha \cos \theta \sin \theta \xi_{\parallel} = 0, \quad (\text{A16})$$

$$(c^2/V_A^2 - \cos^2 \theta) \xi_{\parallel} - \alpha \sin \theta \cos \theta \xi_{\perp} - (\alpha - 1) \cos^2 \theta \xi_{\parallel} = 0. \quad (\text{A17})$$

Rearranging these, we get

$$(c^2/V_A^2 - \alpha \sin^2 \theta - 1) \xi_{\perp} - \alpha \cos \theta \sin \theta \xi_{\parallel} = 0, \quad (\text{A18})$$

$$(c^2/V_A^2 - \alpha \cos^2 \theta) \xi_{\parallel} - \alpha \sin \theta \cos \theta \xi_{\perp} = 0. \quad (\text{A19})$$

Combining these two, we get

$$(c^2/V_A^2 - \alpha \sin^2 \theta - 1)(c^2/V_A^2 - \alpha \cos^2 \theta) = \alpha^2 \sin^2 \theta \cos^2 \theta. \quad (\text{A20})$$

Therefore, the dispersion relation is

$$c^4/V_A^4 - (1 + \alpha)c^2/V_A^2 + \alpha \cos^2 \theta = 0. \quad (\text{A21})$$

The roots of the equation are

$$c_{f,s}^2 = \frac{1}{2} V_A^2 \left[(1 + \alpha) \pm \sqrt{(1 + \alpha)^2 - 4\alpha \cos^2 \theta} \right], \quad (\text{A22})$$

where subscripts ‘f’ and ‘s’ stand for ‘fast’ and ‘slow’ waves, respectively.

We can write

$$\xi = \xi_{\parallel} \hat{\mathbf{k}}_{\parallel} + \xi_{\perp} \hat{\mathbf{k}}_{\perp} \propto \left[\frac{\xi_{\parallel} k_{\perp}}{\xi_{\perp} k_{\parallel}} \right] k_{\parallel} \hat{\mathbf{k}}_{\parallel} + k_{\perp} \hat{\mathbf{k}}_{\perp}. \quad (\text{A23})$$

Plugging eq. (A22) into eq. (A18) and (A19), we get

$$\left[\frac{1 + \alpha}{2} \pm \frac{\sqrt{D}}{2} - \alpha \sin^2 \theta - 1 \right] \xi_{\perp} = \alpha \cos \theta \sin \theta \xi_{\parallel}, \quad (\text{A24})$$

$$\left[\frac{1 + \alpha}{2} \pm \frac{\sqrt{D}}{2} - \alpha \cos^2 \theta \right] \xi_{\parallel} = \alpha \cos \theta \sin \theta \xi_{\perp}, \quad (\text{A25})$$

where $D = (1 + \alpha)^2 - 4\alpha \cos^2 \theta$. Using $k_{\parallel} = k \cos \theta$ and $k_{\perp} = k \sin \theta$, we get

$$\left[\frac{-1 + \alpha}{2} \pm \frac{\sqrt{D}}{2} \right] \xi_{\perp} k_{\parallel} - \alpha \sin^2 \theta \xi_{\perp} k_{\parallel} = \alpha \cos^2 \theta \xi_{\parallel} k_{\perp}, \quad (\text{A26})$$

$$\left[\frac{1 + \alpha}{2} \pm \frac{\sqrt{D}}{2} \right] \xi_{\parallel} k_{\perp} - \alpha \cos^2 \theta \xi_{\parallel} k_{\perp} = \alpha \sin^2 \theta \xi_{\perp} k_{\parallel}, \quad (\text{A27})$$

Arranging these, we get

$$\frac{\xi_{\parallel} k_{\perp}}{\xi_{\perp} k_{\parallel}} = \frac{-1 + \alpha \pm \sqrt{D}}{1 + \alpha \pm \sqrt{D}}, \quad (\text{A28})$$

where the upper signs are for fast mode and the lower signs for slow mode. Therefore, we get

$$\hat{\xi}_s \propto (-1 + \alpha - \sqrt{D}) k_{\parallel} \hat{\mathbf{k}}_{\parallel} + (1 + \alpha - \sqrt{D}) k_{\perp} \hat{\mathbf{k}}_{\perp}, \quad (\text{A29})$$

$$\hat{\xi}_f \propto (-1 + \alpha + \sqrt{D}) k_{\parallel} \hat{\mathbf{k}}_{\parallel} + (1 + \alpha + \sqrt{D}) k_{\perp} \hat{\mathbf{k}}_{\perp}. \quad (\text{A30})$$

The slow basis $\hat{\xi}_s$ lies between $\hat{\mathbf{k}}_{\parallel}$ and $-\hat{\theta}$. The slow basis $\hat{\xi}_f$ lies between $\hat{\mathbf{k}}_{\perp}$ and $\hat{\mathbf{k}}$ (Fig. 1). Here overall sign of $\hat{\xi}_s$ and $\hat{\xi}_f$ is not important.

When $\alpha \rightarrow 0$, equations (A30) and (A29) becomes

$$\hat{\xi}_s \approx \hat{\mathbf{k}}_{\parallel} - (\alpha \sin \theta \cos \theta) \hat{\mathbf{k}}_{\perp}, \quad (\text{A31})$$

$$\hat{\xi}_f \approx (\alpha \sin \theta \cos \theta) \hat{\mathbf{k}}_{\parallel} + \hat{\mathbf{k}}_{\perp}. \quad (\text{A32})$$

In this limit, $\hat{\xi}_s$ is mostly proportional to $\hat{\mathbf{k}}_{\parallel}$ and $\hat{\xi}_f$ to $\hat{\mathbf{k}}_{\perp}$. When $\alpha \rightarrow \infty$, equations (A30) and (A29) becomes

$$\hat{\xi}_s \approx -\hat{\theta} + (\sin \theta \cos \theta / \alpha) \hat{\mathbf{k}}, \quad (\text{A33})$$

$$\hat{\xi}_f \approx (\sin \theta \cos \theta / \alpha) \hat{\theta} + \hat{\mathbf{k}}. \quad (\text{A34})$$

When $\alpha = \infty$, slow modes are called *pseudo*-Alfvénic modes.

We can obtain slow and fast velocity component by projecting Fourier velocity component $\mathbf{v}_{\mathbf{k}}$ onto $\hat{\xi}_s$ and $\hat{\xi}_f$, respectively.

To separate slow and fast magnetic modes, we assume the linearized continuity equation ($\omega \rho_{\mathbf{k}} = \rho_0 \mathbf{k} \cdot \mathbf{v}_{\mathbf{k}}$) and the induction equation ($\omega \mathbf{b}_{\mathbf{k}} = \mathbf{k} \times (\mathbf{B}_0 \times \mathbf{v}_{\mathbf{k}})$) are *statistically* true. From these, we get Fourier components of density and *non-Alfvénic* magnetic field:

$$\begin{aligned} \rho_{\mathbf{k}} &= (\rho_0 \Delta v_{k,s}/c_s) \hat{\mathbf{k}} \cdot \hat{\xi}_s + (\rho_0 \Delta v_{k,f}/c_f) \hat{\mathbf{k}} \cdot \hat{\xi}_f \\ &\equiv \rho_{k,s} + \rho_{k,f}, \end{aligned} \quad (\text{A35})$$

$$\begin{aligned} b_{\mathbf{k}} &= (B_0 \Delta v_{k,s}/c_s) |\hat{\mathbf{B}}_0 \times \hat{\xi}_s| + (B_0 \Delta v_{k,f}/c_f) |\hat{\mathbf{B}}_0 \times \hat{\xi}_f| \\ &\equiv b_{k,s} + b_{k,f}, \end{aligned} \quad (\text{A36})$$

$$\begin{aligned} &= \rho_{k,s} (B_0/\rho_0) (|\hat{\mathbf{B}}_0 \times \hat{\xi}_s|/\hat{\mathbf{k}} \cdot \hat{\xi}_s) \\ &+ \rho_{k,f} (B_0/\rho_0) (|\hat{\mathbf{B}}_0 \times \hat{\xi}_f|/\hat{\mathbf{k}} \cdot \hat{\xi}_f), \end{aligned} \quad (\text{A37})$$

where $\Delta v_{\mathbf{k}} \propto v_{\mathbf{k}}^+ - v_{\mathbf{k}}^-$ (superscripts ‘+’ and ‘-’ represent opposite directions of wave propagation) and subscripts ‘s’ and ‘f’ stand for ‘slow’ and ‘fast’ modes, respectively. From equations (A35), (A36), and (A37), we can obtain $\rho_{k,s}$, $\rho_{k,f}$, $b_{k,s}$, and $b_{k,f}$ in Fourier space.

APPENDIX B: SCALE-DEPENDENT ANISOTROPY

Fig. B1a shows the shapes of Alfvén eddies of different sizes. Left 3 panels show an increased anisotropy as we move from the top (large eddies) to the bottom (small eddies). The horizontal axes of the left panels are parallel to \mathbf{B}_0 . Structures in the perpendicular plane (right panels) do not show a systematic elongation. However, Fig. B1b shows that velocity of fast modes exhibit isotropy. Data are from a simulation with 216^3 grid points, $M_s = 2.3$, and $\beta = 0.2$.

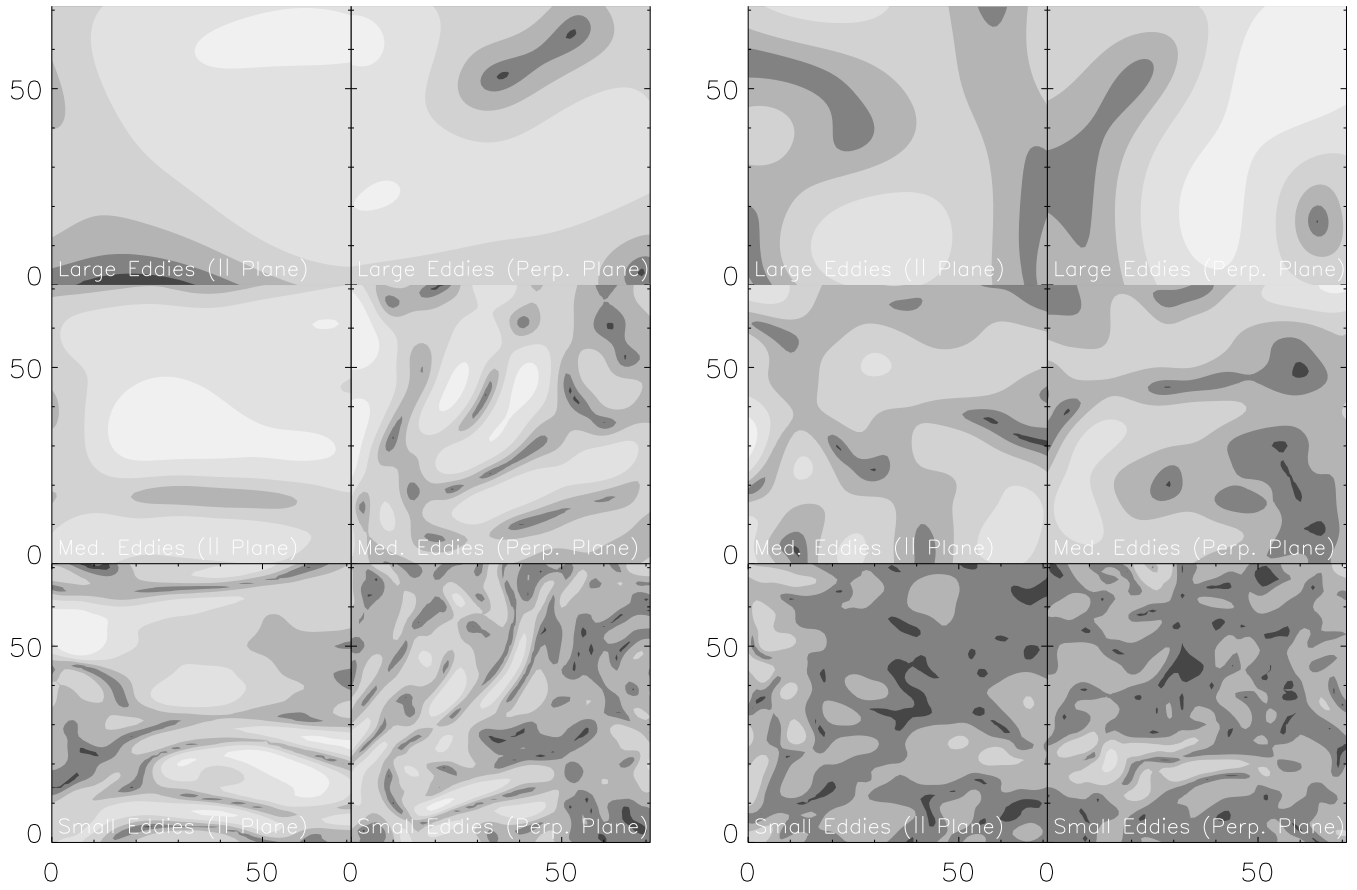


Figure B1. Anisotropy as a function of scale. (*Left*) Alfvén mode velocity show scale-dependent anisotropy. (*Right*) Fast mode velocity show isotropy. Only part of the data cube is shown. Lighter tones are for larger $|\mathbf{v}|$. Magnetic field show similar behaviors.